Computer Models for Wind Flow over Mesoscale Mountainous Terrain Applied to the Yukon

EAS 521 – Final Report submitted: December 17, 1999
By: JP Pinard
Course supervisor: John D. Wilson

1 Introduction

Wind power is the fastest growing source of new energy in the world today. In the Yukon, new wind turbine generators are presently meeting the growing energy demand. The land that is available for wind farm development, however, is often hilly and mountainous. The feasibility of wind energy in such complex terrain requires numerous expensive wind-monitoring stations and often takes several years to properly assess. Wind flow modelling using computer simulation techniques can drastically reduce costs and time.

The present scope of study is to find the most appropriate modelling technique to simulate realistic wind flow over mountainous terrain. This requires an understanding of the relative scale and complexity of the terrain and the ability for a modelling technique to handle them. The landscape in the Yukon where wind energy exploitation is feasible is made up of mountainous terrain in the order of 500 to 1000 m in height and 2 to 10 km in length. Distances between mountains are about 5 to 20 km. The appropriate domain size would therefore be about 10 to 100 km.

The domain size just described helps suggest what influences may be important, which then helps us in finding the appropriate type of model. Microscale models are designed for small, gently sloped hills of the order 100 m above a flat plain. Most of these models do not handle Coriolis or buoyancy effects. The mesoscale models, however, have been developed with the ability to handle complex terrain, Coriolis, thermodynamic fluxes and turbulence. The latter models were designed for much larger terrain and for time-dependant, or prognostic modelling in weather prediction. But it is also possible that these models are capable of handling smaller scale terrain effect such as described above.

The purpose of this discussion is to explore the suitability of existing computer models in assessing wind energy potential over complex terrain. This study has two components: one is a review of the theory and applicability of currently available techniques. The other component is a test of the RAMS (Region Atmospheric Modelling System) mesoscale model, which is presently installed at the Northern Forestry Centre[1] in Edmonton. The RAMS model version 3b is being used to simulate a wind flow over real complex terrain on a domain size of 25 by 25-km.

[1] The author would like to thank Richard Carr, Peter Englefield, Kerry Anderson, and the Northern Forestry Centre in Edmonton, who have generously provided the assistance and computer usage to carry out the RAMS experimentation

Included in the appendices is a historical overview of the microscale models, an investigation comparing six mesoscale models, a list of web sites providing information on the mesoscale models, and the parameter list for the RAMS model simulation.

2 Theory

The planetary boundary layer (PBL) is the portion of the atmosphere that is highly turbulent and strongly influenced by the effects of the Earth's surface on a relatively short time scale (order of hours) (Holton, 1992). In the free atmosphere above the PBL the turbulence can be ignored in an approximate treatment of the synoptic-scale motions. The focus of the model treatment is on the PBL and its turbulent mixing.

2.1 Flow Models

2.1.1 Flat Plain

In a simple study of a microscale steady state wind flow within the PBL, the "reference flow" or "basic state" is a wind flow over a flat plain. The reference state is usually one-dimensional with a ground-zero vertical z-axis. The flow is slowed down by the drag exerted near the ground. The scale of the surface irregularity (z_o, the surface roughness length) plays a role in defining the shape of the vertical wind profile that results from the ground drag. This profile can be represented by $\bar{u}_o(z)$ and is logarithmic for a deep, ground-based layer of the neutrally stratified PBL. Allowing for stratification, the vertical wind speed profile can be represented by

$$\bar{u}_0(z) = \left(\frac{u_*}{\kappa}\right)\left[\ln\left(\frac{z}{z_o}\right) - \psi\left(\frac{z}{L}\right) + \psi\left(\frac{z_0}{L}\right)\right] \qquad (2.1)$$

where $\bar{u}_0(z)$ is the wind speed at height z above ground surface. The friction velocity u_* is related to the surface stress τ through the definition $|\tau| = \rho u_*^2$ (ρ is the air density). The von Kármán constant κ is usually taken as 0.40 (Justus, 1978). The parameter L is called the Monin-Obukhov length and ψ is a universal dimensionless flow (or model) profile function (Paulson, 1970) which depends on the atmospheric stability.

2.1.2 Two-dimensional Hill

A two-dimensional hill is introduced into the model, and the air is now forced to flow over that hill. The shape of the profile of horizontal (or terrain-following) speed wind changes, as the air moves over the hill. Figure 1 shows a simple hill and defines some of the key scales controlling hill flows.

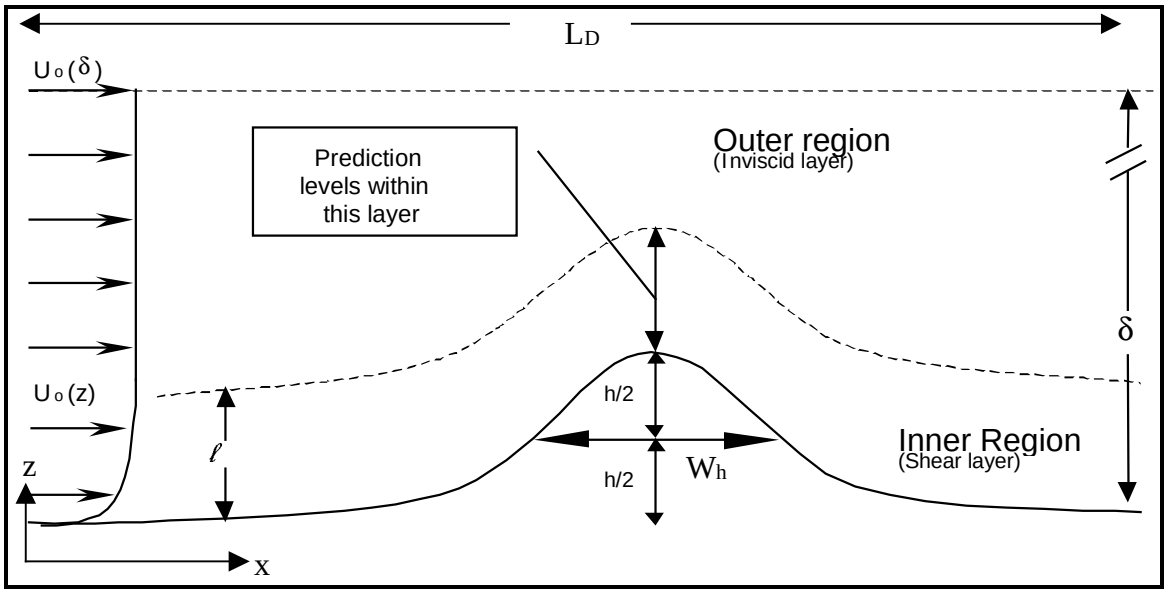

Figure 1 - Flow over Hill

L_D denotes the domain size. The variable W_h is the length of the hill, measured at half the height h of the hill. In the linear theory of Hunt et al. (1988a), the PBL above a hill is divided into an inner and an outer region. In the inner region (height *l*) the shear stress or turbulent friction exerts an important influence on the mean flow, whereas in the outer region (height δ) the flow is defined as an inviscid potential flow dominated by inertial forces. Stratification is of course likely to be important (Hunt et al., 1988), unless the approach flow is neutrally-stratified.

In the linear approach to be discussed in Section 3.2 we can describe the changing wind flow with a background horizontal wind profile $\bar{u}_0(z)$ on which we super-impose a disturbance denoted by $\hat{u}$,

$$\bar{u}(x,z) = \bar{u}_0(z) + \hat{u}(x,z) \qquad (2.2)$$

If terms in $\hat{u}^2$ are neglected, this type of flow can be solved analytically.

2.1.3 Three-dimensional Hill

A third dimension is added to the model, and the hill becomes an isolated protrusion above a flat plain. This now introduces an allowance for air to flow above and around the hill. It also adds more complexity to the equations used in the model. The analytical (linearised) solution remains straightforward.

The dimensionless Froude number is a simple way to help understand the effects of buoyancy on airflow over a simple hill (refer to **Figure 2**). In the simplest form, Froude number (F_r) can be defined as

$$F_r^2 = \frac{\text{Inertial forces}}{\text{Bouyant forces}} \qquad (2.3)$$

The inertial forces (order $\bar{u}_0^2/W_h$) act in the horizontal direction along the wind flow, and the buoyant forces (order $g\frac{\Delta\theta}{\theta_0}$ where $\Delta\theta$ is a typical temperature disturbance, g is gravitational acceleration, θ_0 is potential temperature) act in the vertical. The Froude number can be more elaborately defined as

$$F_r^2 = \frac{\bar{u}_0^2 / W_h}{g\Delta\theta/\theta_0}. \qquad (2.4)$$

The Brunt-Väisälä frequency is a time scale related to the natural period of oscillation (in the form of gravity waves) of a parcel in a statically stable atmosphere. It is given by

$$N^2[s^{-2}] = \frac{g}{\theta_0}\frac{\partial\theta}{\partial z} \approx \frac{g}{\theta_0}\frac{\Delta\theta}{h} \qquad (2.5)$$

Substituting equation (2.5) into (2.4), results in the following,

$$F_r^2 = \frac{\bar{u}_0^2}{N^2 W_h h}, \text{ or } \quad F_r = \frac{\bar{u}_0}{N\sqrt{W_h h}} \qquad (2.6)$$

For a strongly stable environments, i.e. where the buoyancy affects are strong, and Fr ≈ 0.1 the air flows around the hill (**Figure 2** (a)) and a stagnant mass of air builds up before the hill.

At a slightly faster wind (Fr ≈ 0.4) some of the air flows over the hill (**Figure 2** (b)) while the air at lower altitudes separate to flow around the hill. The natural wavelength of the air that flows over the top is much smaller than the hill size and the flow is perturbed by the hill to form lee waves. A lee wave separation occurs from the top and flows above the air that flows around the hill. A column of air with the same height as the hill approaches the hill and a fraction of it flows above the hill.

At higher wind speeds and Fr ≈ 1.0, the stability is weaker and the wavelength of the gravity waves (lee waves) approaches the size of the hill (**Figure 2** (c)). A natural resonance forms the large amplitude lee waves or mountain waves. If there is sufficient moisture, lenticular clouds can form along the crests of the waves downstream of the hill.

For stronger winds with Fr ≈ 1.7 (**Figure 2** (d)) the natural wavelength is longer than the hill dimensions, thus causing a boundary layer separation at the lee of the hill.

Neutral stratification (**Figure 2** (e)) occurs for strong winds with neutral stability (no convection) and Froude number approaching infinity. The streamlines are disturbed upwind and above the hill out to a distance of about 3 times the hill length W_H. Near the top of the hill the streamlines are packed closer together, causing a speed-up of the wind.

Immediately downwind of the hill is often a cavity associated with boundary layer separation (Tampieri, 1987). This is the start of a turbulent wake behind the hill. The height of the turbulent wake is initially the same order as the size of the hill and grows in size and diminishes in turbulent intensity downwind. Eventually the turbulence decays and the wind flow returns to its undisturbed state.

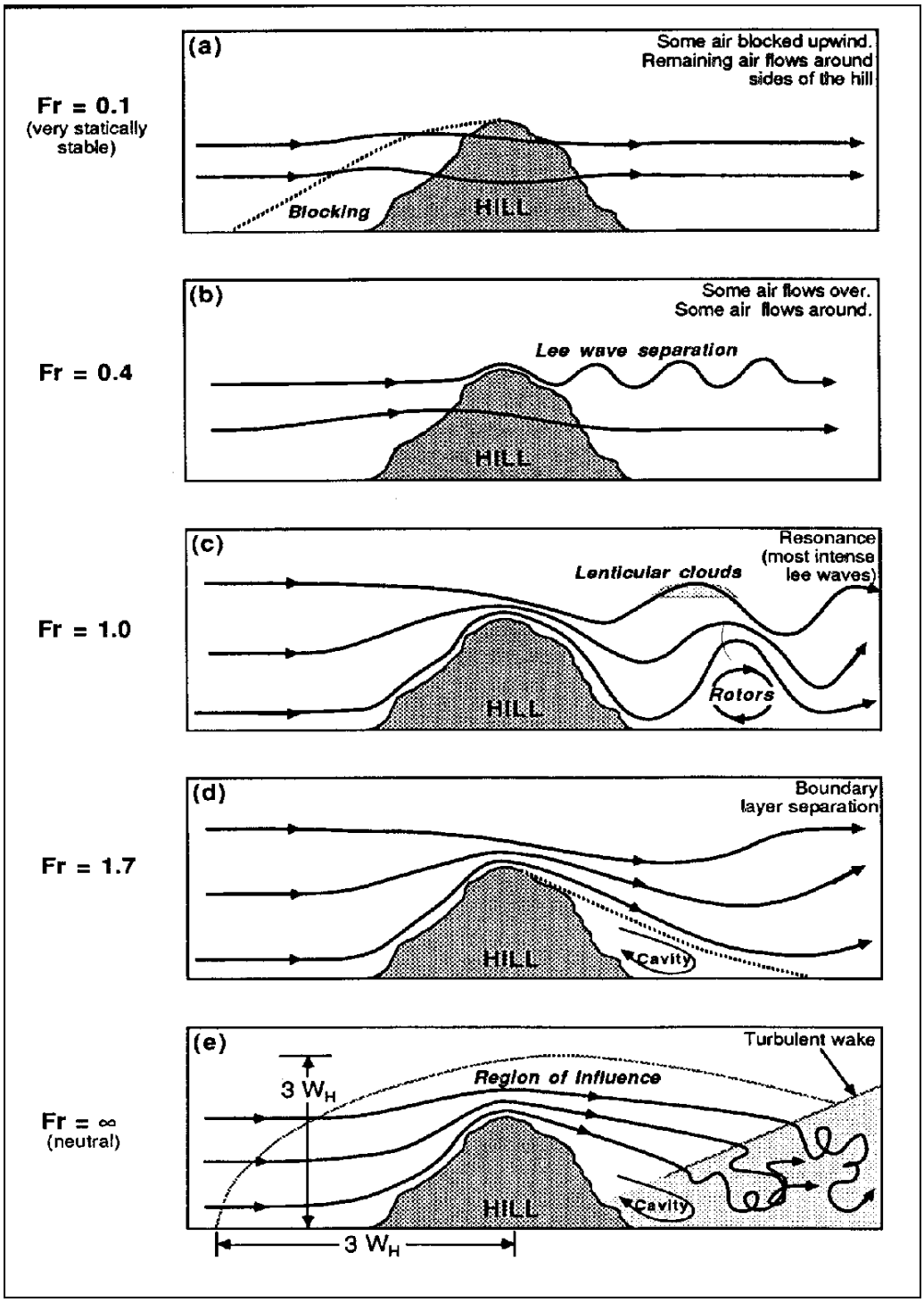

Figure 2- Flow over isolated hill with Froude number variation (Source: Stull, 1988)

2.1.4 Complex Terrain

A more complex situation would be terrain having elongated mountains with heterogeneous shapes, surrounded by other mountains. This begins to fall under a "mesoscale" class, where the appropriate domain size L_d is of order 10-100 km or more. The Coriolis effect (denoted by f[2], due to the Earth's rotation) is now important because the "domain crossing time" $L_d/\bar{u}_0 \not< f^{-1}$.

Hunt et al. (1990) suggested three conditions in which hilly terrain can fall under a mesoscale class. The first is having a "long" passage time over the domain, i.e. a small Rossby number $R_o = \bar{u}/(fL_D)$ (≈ 0.1 where $L_D \approx 100$ km, $\bar{u} \approx 10$ m/s, and $f \approx 10^{-4}$). The second is the case where gravity waves set up by the flow are of dominant importance. Individual land features with height h (≈ 500 m for a hill) can disturb flow over a long distance (domain size) $L_D \approx hN/f$ (≈ 50 km). And the third scenario is a cumulative effect of many hills of scale W_h distributed over a distance $L_D >> W_h$.

If we choose the hill to be $W_h \approx 1000$ m long We can use the Froude number defined by Equation (2.6) to derive values

$$F_r = \frac{\bar{u}_0}{N\sqrt{W_h h}} = \frac{10}{10^{-2}\sqrt{1000 \times 500}} \approx 1.4$$

which indicates strong lateral inertial forces over buoyancy. Thus wind is likely to flow over the top of the mountain, natural wavelength become longer than the hill dimension, and boundary layer separation occur at the lee of the hill.

2.2 Basic Equations under Boussinesq Approximation

Within the PBL a set of governing equations need to be derived that account for the effects of turbulence. The important equations are those for conservation of mass, momentum, and heat. These could be derived in their full form and complexity, but it is found not to be necessary when applied to the PBL.

The basic state density in the lowest kilometre of the atmosphere (PBL) varies by only about 10%, and its fluctuating component varies by only a few percent. The Boussinesq approximation assumes that the variations in the density affect the buoyancy term, but may be neglected in the inertial terms of the momentum equations. For the small amplitudes of vertical displacements that are expected in flow over hills, the Boussinesq approximation is always valid (Kaimal and Finnigan, 1994).

[2] $f = 2\Omega\sin\phi$, where ϕ = latitude on Earth, $\Omega = 2\pi/24x60x60$ rad/s. At mid-latitudes $f \sim 10^{-4}$ s^{-1}.

2.2.1 Conservation of Mass

The rigorous statement for conservation of mass is expressed by

$$\frac{\partial \rho}{\partial t} + \frac{\partial \rho u}{\partial x} + \frac{\partial \rho v}{\partial y} + \frac{\partial \rho w}{\partial z} = 0 \qquad (2.6)$$

Where ρ is the air density and u, v, and w are the wind speed in the Cartesian system defined by x, y, and z, where z is the vertical co-ordinate.

Under the Boussinesq approximation the continuity equation simplifies to a statement that the velocity field is non-divergent,

$$\nabla \cdot u_i = \frac{\partial u_i}{\partial x_i} = \frac{\partial u}{\partial x} + \frac{\partial v}{\partial y} + \frac{\partial w}{\partial z} \qquad (2.7)$$

The symbol u_i represents the vector velocity, i.e. $u_i = (u_1,u_2,u_3) = (u,v,w)$. The grad operator ∇ is shorthand for $\partial / \partial x_i$.

For an atmospheric layer or motion much deeper that the PBL, such as a cumulonimbus cloud, the Boussinesq approximation is unrealistic. Mean density gradients are non-negligible, and essential for properly representing buoyancy force. Thus we have a relation known as the **deep convection continuity equation** (Pielke, 1984)

$$\frac{\partial}{\partial x_j}(\rho_0 u_j) = 0 \qquad (2.8)$$

This more complex statement of mass conservation is necessary if the vertical depth of circulation is on the same order as the density scale depth. The parameter $\rho_0 = \rho_0(x,y,z)$ is defined as a synoptic scale reference, or temporally constant mean, density. Most often ρ_0 is regarded as ranging only in the vertical, $\rho_0 = \rho_0(z)$. This form of the conservation-of-mass relation eliminates sound waves (Pielke, 1984) as a possible solution and can be referred to as the anelastic, or soundproof, assumption.

2.2.2 Conservation of Momentum

The equations of motion under the Boussinesq approximation are

$$\frac{Du}{Dt} = \frac{\partial u}{\partial t} + u\frac{\partial u}{\partial x} + v\frac{\partial u}{\partial y} + w\frac{\partial u}{\partial z} = -\frac{1}{\rho_0}\frac{\partial p}{\partial x} + fv + \nu\nabla^2 u \qquad (2.9)$$

$$\frac{Dv}{Dt} = \frac{\partial v}{\partial t} + u\frac{\partial v}{\partial x} + v\frac{\partial v}{\partial y} + w\frac{\partial v}{\partial z} = -\frac{1}{\rho_0}\frac{\partial p}{\partial y} - fu + \nu\nabla^2 v \qquad (2.10)$$

$$\frac{Dw}{Dt} = \frac{\partial w}{\partial t} + u\frac{\partial w}{\partial x} + v\frac{\partial w}{\partial y} + w\frac{\partial w}{\partial z} = -\frac{1}{\rho_0}\frac{\partial p}{\partial z} - g\frac{\theta}{\theta_0} + \nu\nabla^2 w \qquad (2.11)$$

Here ρ_o is a constant mean value for density. Other variables are the pressure departure from a hydrostatic state p, the Coriolis parameter *f*, the gravitational acceleration g, the departure of potential temperature θ from its basic state θ_o, and the kinematic viscosity ν. Viscous friction can usually be neglected.

2.2.3 Conservation of Heat

The thermodynamic energy equation has the form

$$\frac{D\theta}{Dt} = \frac{\partial\theta}{\partial t} + u\frac{\partial\theta}{\partial x} + v\frac{\partial\theta}{\partial y} + w\frac{\partial\theta}{\partial z} = \kappa\nabla^2\theta + S_\theta \qquad (2.12)$$

S_θ represents the sources and sinks of heat including freezing and melting, condensation and evaporation, deposition and sublimation, radiative divergence, etc. The term κ is the molecular thermal diffusivity, and $\kappa\nabla^2\theta$ is the divergence of the molecular heat flux.

Because molecular transfer of heat (through diffusion) or other properties of the air is very small relative to exchange by the motion of fluid, we usually set the right hand side to zero.

2.3 Reynolds Averaging and Turbulence Closures

The atmosphere is a continuum, in motion on a vast range of length scales. We will never have a clear knowledge of state of motion at every point at every instant. So it becomes necessary to define "resolved" and "unresolved" scales of motion, and to approximate the influence of the unresolved scales on the resolved. For example, let's consider the velocity component u_i. It can be decomposed into the sum of the average $\bar{u}_i$ and the deviation from the average u_i', i.e. $u_i = \bar{u}_i + u_i'$. The average is the resolved component and the deviation (also known as the "fluctuation") is the unresolved component.

The unresolved field plays an important role in the evolution of the average; i.e. it will change the average over time. Parameterisation of that influence is the role of a "closure model", which is formulated in terms of statistics of u_i'. In the first order closure, the influence of the unresolved turbulence eddies is treated as equivalent to an increased viscosity of the fluid. In contrast, a higher order closure consists of a set of differential equations for statistics of the unresolved motion, these being derived from the Navier-Stokes equation themselves.

The averaged form of the conservation equations is obtained by substituting $u_i = \bar{u}_i + u_i'$ and averaging. The resulting equations are:

$$\frac{\partial\overline{u_i}}{\partial x_i} = \frac{\partial\overline{u}}{\partial x} + \frac{\partial\overline{v}}{\partial y} + \frac{\partial\overline{w}}{\partial z} = 0 \qquad (2.13)$$

$$\frac{\partial \overline{u}}{\partial t}+\overline{u}\frac{\partial \overline{u}}{\partial x}+\overline{v}\frac{\partial \overline{u}}{\partial y}+\overline{w}\frac{\partial \overline{u}}{\partial z}=-\frac{1}{\rho_0}\frac{\partial \overline{p}}{\partial x}+f\,\overline{v}-\left[\frac{\partial \overline{u'u'}}{\partial x}+\frac{\partial \overline{u'v'}}{\partial y}+\frac{\partial \overline{u'w'}}{\partial z}\right] \quad (2.14)$$

$$\frac{\partial \overline{v}}{\partial t}+\overline{u}\frac{\partial \overline{v}}{\partial x}+\overline{v}\frac{\partial \overline{v}}{\partial y}+\overline{w}\frac{\partial \overline{v}}{\partial z}=-\frac{1}{\rho_0}\frac{\partial \overline{p}}{\partial y}+f\,\overline{u}-\left[\frac{\partial \overline{\overline{v}u'}}{\partial x}+\frac{\partial \overline{\overline{v}v'}}{\partial y}+\frac{\partial \overline{\overline{v}w'}}{\partial z}\right] \quad (2.15)$$

$$\frac{\partial \overline{w}}{\partial t}+\overline{u}\frac{\partial \overline{w}}{\partial x}+\overline{v}\frac{\partial \overline{w}}{\partial y}+\overline{w}\frac{\partial \overline{w}}{\partial z}=-\frac{1}{\rho_0}\frac{\partial \overline{p}}{\partial z}+g\frac{\overline{\theta}}{\theta_0}-\left[\frac{\partial \overline{w'u'}}{\partial x}+\frac{\partial \overline{w'v'}}{\partial y}+\frac{\partial \overline{w'w'}}{\partial z}\right] \quad (2.16)$$

$$\frac{\partial \overline{\theta}}{\partial t}+\overline{u}\frac{\partial \overline{\theta}}{\partial x}+\overline{v}\frac{\partial \overline{\theta}}{\partial y}+\overline{w}\frac{\partial \overline{\theta}}{\partial z}=-\overline{w}\frac{\partial \theta_0}{\partial z}-\left[\frac{\partial \overline{\theta'u'}}{\partial x}+\frac{\partial \overline{\theta'v'}}{\partial y}+\frac{\partial \overline{\theta'w'}}{\partial z}\right] \quad (2.17)$$

The terms in the square brackets represent the influence of the unresolved scales on the resolved flow ($\bar{u}_i$, $\overline{\theta}$), and mathematically have the form of spatial gradients of various turbulence covariances. For example, $R_{ij} = \overline{u_i' u_j'}$ is the Reynolds stress tensor (shear stress, momentum flux).

The effects of the unresolved scales, i.e. the unknown terms in brackets, need to be accounted for by some approximation (a "turbulence closure scheme").

2.3.1 First-Order Closure

The K-theory is one such turbulence closure scheme. It is a first-order closure that relates the velocity gradient to the shear stress. In its fullest form K-theory has correct tensor symmetry, i.e.

$$\overline{u_i' u_j'} = -K_m\left(\frac{\partial \overline{u_i}}{\partial x_j}+\frac{\partial \overline{u_j}}{\partial x_i}\right) \quad (2.18)$$

The most familiar component $\overline{u'w'}$ is given by

$$\overline{u'w'} = -K_m\left(\frac{\partial \overline{u}}{\partial z}+\frac{\partial \overline{w}}{\partial x}\right) \quad (2.19)$$

The K-theory represents turbulent convection by the unresolved scales as if it were a diffusive process.

2.3.2 Higher Order Closure

Higher-order closures appeal to the Navier-Stokes equations themselves to obtain exact governing equations for the turbulence statistics ($\overline{u_i' u_j'}$), which are subsequently simplified so as to attain closure (as many equations as unknowns). These equations are quite complex, and a single example will be given, that of the streamwise variance $\overline{u'^2} = \sigma_u^2$ in a flow with y-symmetry:

$$\begin{aligned}
\frac{\partial \overline{u'^2}}{\partial t} + \bar{u}\frac{\partial \overline{u'^2}}{\partial x} + \bar{w}\frac{\partial \overline{u'^2}}{\partial z} &= -2\,\overline{u'^2}\,\frac{\partial \bar{u}}{\partial x} - 2\,\overline{u'w'}\,\frac{\partial \bar{u}}{\partial z} && \text{shear production} \\
&\quad -\frac{\partial}{\partial x}(\overline{u'u'u'}) - \frac{\partial}{\partial z}(\overline{w'u'u'}) && \text{turbulent transport} \\
&\quad -\frac{2}{\rho_0}\overline{u'\frac{\partial p'}{\partial x}} && \text{pressure transport} \\
&\quad + \text{other terms}
\end{aligned} \qquad (2.20)$$

Note that many mechanisms are resolved exactly by a second-order closure, e.g. advection of variance $\bar{u}\,\partial\overline{u'^2}/\partial x$ and the shear production of variance (e.g. $\overline{u'w'}\,\partial\bar{u}/\partial z$). Other mechanisms have to be approximated, for example the triple moments $\overline{u_i' u_j' u_k'}$ are often assumed to be fluxes driven by spatial gradients in $\overline{u_i' u_j'}$; an eddy diffusivity of second order (K^{2O}) is introduced, e.g.

$$\overline{w'u'u'} = -K^{20}\frac{\partial \overline{u'^2}}{\partial z}. \qquad (2.21)$$

3 A Family of Hill Flow Models

Figure 3 delineates the various categories of hill flow models. The principal division is that between the steady state and time-dependant treatments. The steady-state models are appropriate to resolve the time average flow and turbulence statistics if the flow over the terrain can be regarded as stationary (statistics invariant in time).

Generally this requires that the region of hilly terrain be small enough that the passage of time $L_D/\bar{u}_0(\delta)$ (i.e. 25 km/10 m/s ≈ 42 minutes) be much smaller than the time (Γ, order of 60 minutes) over which "external" conditions (approach wind direction; solar elevation; mesoscale disturbance; etc…) evolve significantly. Thus, to describe real flow over a large domain of hills (say, L_D order 10-100 km i.e. mesoscale), it is usually appropriate to retain time-dependence[3]. One may also choose to resolve some of the large eddies (LES) in microscale flow.

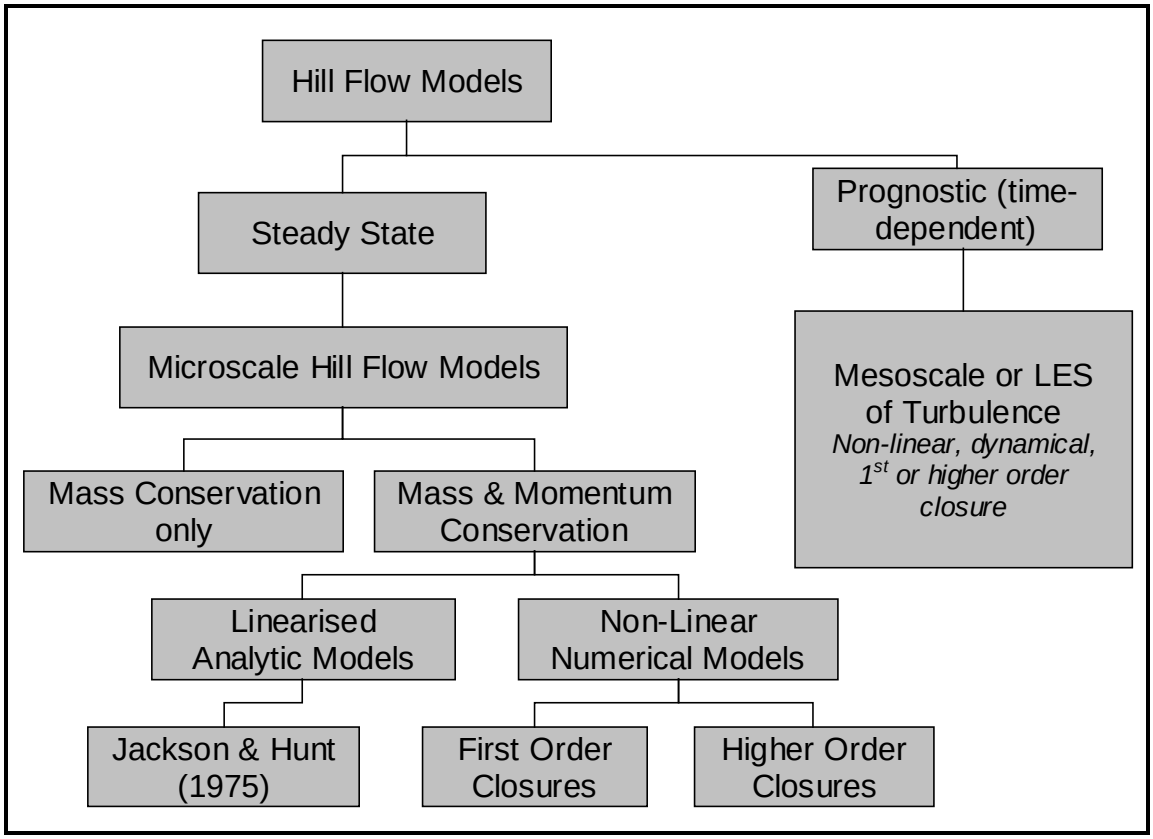

Figure 3 - Flow diagram showing the family tree of atmospheric flow models

Four groups have been identified in computer modelling techniques developed for flow over hills. Those groups are mass consistent models, the linearised dynamical models, the

[3] An exception might be the study of an idealised condition where inflow winds, and thermal stability were held constant with the object of diagnosing a putative steady state flow pattern.

non-linearised dynamical models and the prognostic models. Each of these main groups is described below, giving reference to particular products developed by institution or company.

3.1 Mass Consistent Model

Mass-consistent models seek to find a divergence-free wind velocity field that departs by the smallest possible amount from some initial wind field derived from observations. The adjustment needed to achieve zero divergence is determined through an iterative solution of a set of the continuity equations. A discrete (possibly finite-element) mesh is set up throughout the region of interest, and the key variables are defined at the centres or faces of each grid cell. The field is then adjusted at each point until the divergence is reduced below a tolerance level.

Mass-consistent models are most applicable in complex terrain where the wind is moderate to strong. In these cases the topography is the main forcing factor on the wind, channelling the flow, or causing it to flow over the hilltops. There can be some input into the type of flow that occurs, i.e. over the topography or around it by specifying horizontal and vertical "transmissivities". A high horizontal transmissivity constrains the flow to be mainly horizontal. This effectively allows for the stable stratification of the atmosphere above the boundary layer. Corrections in the flow field are restricted mainly to the horizontal components of the wind. However this can be an over simplification in very high mountains when the effect of the topography extends high into the troposphere as turbulence and waves.

An example of a mass-conserving model is WindMap[4], which is based on NOABL[5], a program original developed in the 1970s by the U.S. Department of Energy. Another example is NUATMOS[6], which is a wind profile simulation program for use with GIS databases.

The mass conservation model has been shown to perform equally well compared to the JH75 model under real conditions, with typical errors between prediction and measurement of 8 to 10 percent. Such comparisons suggest[7] that conservation of mass is the primary determinant of variations in wind speed over moderately complex terrain.

3.2 Linearised Dynamical Models

In describing the linear theory of hill flows (JH75) we shall establish some basic equations of motion to describe the atmospheric flow and how they are simplified to meet the objective of quantifying the variables in the flow. For simplicity we consider steady state flow with spatial symmetry in y (i.e. an infinite ridge). The mean along wind velocity $\bar{u}(x,z)$ is governed by the time-averaged Navier-Stokes equations, and be written:

[4] Maintained by Brower & Company, Andover, MA, USA
[5] Maintained by Science Applications Inc. of La Jolla California (Traci et al. 1978)
[6] Maintained by Dr. George L. Ball, University of Arizona
[7] As stated by the manual for the WindMap programme

$$\frac{\partial \overline{u}}{\partial t} + \overline{u}\frac{\partial \overline{u}}{\partial x} + \overline{v}\frac{\partial \overline{u}}{\partial y} + \overline{w}\frac{\partial \overline{u}}{\partial z} = -\frac{1}{\rho_0}\frac{\partial \overline{p}}{\partial x} - \frac{\partial \overline{u'^2}}{\partial x} - \frac{\partial \overline{u'w'}}{\partial z} \qquad (3.1)$$

where the acceleration term $\partial\overline{u}/\partial t = 0$ by assumption of steady state. The last equation, supplement by closure assumptions to specify the stresses $\overline{u'^2}$, $\overline{u'w'}$, is the heart of any dynamical hill flow model: but it is non-linear, and so impossible to solve analytically.

However, if we decompose the streamwise wind speed $\overline{u}$ (x, z) as a superimposed (steady) disturbance û(x,z) on an approaching equilibrium flow $\overline{u}_o$(z), we have

$$u(x,z) = \overline{u}_0(z) + \hat{u}(x,z), \text{ and } \quad w(x,z) = \overline{w}_0(z) + \hat{w}(x,z) \qquad (3.2)$$

where $\overline{w}_0 = 0$ and, note, $u^2 = \overline{u}_0^2 + 2\overline{u}_0\hat{u} + \hat{u}_0^2$.

Substituting the above into equation (3.1) and knowing that $\overline{u}_o$ is constant in the x-direction, we obtain:

$$\overline{u}_0\frac{\partial \hat{u}}{\partial x} + \hat{u}\frac{\partial \hat{u}}{\partial x} + \hat{w}\frac{\partial \overline{u}_0}{\partial z} + \hat{w}\frac{\partial \hat{u}}{\partial z} = F(\overline{p}, \overline{u'^2}, \overline{u'w'}) \qquad (3.3)$$

This is a quadratic equation for the flow disturbance, in that the second and fourth terms are of second order in the unknown flow disturbance (i.e. non-linear). If we assume that û is much smaller than $\overline{u}_o$ and drop all second order terms, the equation of motion becomes linear in the disturbance

$$\overline{u}_0\frac{\partial \hat{u}}{\partial x} + \hat{w}\frac{\partial \overline{u}_0}{\partial z} = F(\overline{p}, \overline{u'^2}, \overline{u'w'}) \qquad (3.4)$$

and so can be solved using standard methods of applied mathematics. Linearisation is the key to the JH75 theory. Software programmes developed under this theory are MS-Micro/3[8] and WAsP[9].

3.3 Non-Linear Dynamical Models

The non-linear advection terms ($\hat{u}\frac{\partial \hat{u}}{\partial x}$ and $\hat{w}\frac{\partial \hat{u}}{\partial z}$, for example) guarantee failure to find analytic solutions for hill flow, except in the case of hills so gentle (disturbances so small) as to permit linearisation.

But if one can live with numerical solution, then there is no difficulty in handling non-linearity. The advantage of the numerical non-linear approach is the ability to handle hills of arbitrary scale and slope. This allows the added bonus of detailed turbulence closures (unfortunately the addition of detail, such as higher order closure, does not necessarily

[8] It is a descendant (Taylor et al., 1983; Walmsley et al., 1986) of the mainframe model MS3DJH/3R, which is based on theory of Jackson and Hunt (1975) and was simplified and extended to three dimensions by Mason and Sykes (1979)

[9] Wind Atlas Analysis and Application Program, developed by the Department of Meteorology and Wind Energy of Risø National Laboratory in Denmark (Troen and Petersen 1989)

improve the scientific description very much if judged by ability to explain observations). The software built under this premise is MSFD-PC[10].

3.4 Prognostic or Mesoscale Models

The primary reason for the historical development of this scale of model was to demonstrate storm-scale numerical weather prediction and to develop, test, and validate a regional forecast system appropriate for operational, commercial, and research applications. This includes large eddy simulations LES and mesoscale models for study of regional flows. Mesoscale models are mostly equipped with a multitude of options that allow users to fit them to very specific scenarios.

These models are governed by the fully compressible Navier-Stokes equations. The equations include the full time derivatives of all three components of velocity, the mass continuity, thermodynamic, water species mixing ratio continuity, and in some models, conservation of airborne particles. These features make prognostic models applicable to the simulation of an extremely wide spectrum of atmospheric motions such as convective cloud formation, and flow over complex terrain.

The co-ordinate system for these models is terrain-following with a distortion to render the uppermost co-ordinate surface horizontal, for example,

$$\frac{\zeta(X,Y,z)}{H} = \left[\frac{z - h_0(X,Y)}{H - h_0(X,Y)} \right]$$

where H is the top of the model domain (at constant elevation z = H), h_0 is the ground height, X and Y are projected co-ordinates, ζ is the model (terrain following) co-ordinate. Note that ζ is the vertical distance from the surface, i.e. it is not orthogonal to the terrain surface.

The mesoscale models have many other features in common, notably

- ◇ 3-dimensional domain
- ◇ temporal and spatial finite-difference scheme (exclusively?)
- ◇ non-hydrostatic, with hydrostatic option
- ◇ compressible
- ◇ turbulent mixing parameterisation (turbulence closure)
- ◇ grid nesting
- ◇ grid staggering
- ◇ a resolved boundary layer
- ◇ long and short wave radiation
- ◇ surface layer, soil and vegetation parameterisation with features such as sea surface temperature, albedo, roughness length, ice cover, snow cover.

The models adopt a limited-area approach and so demand boundary conditions that typically accommodate inflow and outflow, with some accounting for gravity waves.

[10] Mixed Spectral Finite-Difference for Personal Computer, developed by York University, University of Toronto, and CSIRO.

Generally, the mesoscale models allow for the high-resolution grid spacing (less than 10 km), needed in simulating deep convection or flow over complex terrain.

It is not clear how small a grid size these models are capable of handling, however **Table 1** provides a guideline on the capability of some of the models.

Scale	**Domain Size**	**Resolved Circulation**	**Applicable Model**
Micro-scale	< 2 km	Large turbulent eddies	LES model, MS3DJH/3R
Meso-gamma	2-20 km	Thunderstorm convection, complex terrain flows	Non-hydrostatic (ARPS)
Meso-beta	20-200 km	Land-water, sea breezes	Non-hydrostatic, hydrostatic (MM5, RAMS)
Meso-alpha	200-2000 km	Fronts, low-pressure Systems	Hydrostatic (Eta,AVN)

Table 1 - The mesoscale ranges as defined by Orlanski (1975). Found at the web site: www.arl.noaa.gov/slides/ready/local/local2.html

The model ARPS has been used to grid sizes of 200 m and may possibly be used for less than 100 m[11].

Appendix B – Mesoscale Models compares mesoscale models by their capabilities in a table format.

[11] Correspondence by email with Richard Carpenter, U of Oklahoma/CAPS and Daniel B. Weber, CAPS, 1999.

4 RAMS Model Simulation

The RAMS model is a sophisticated package in that it offers many options for the user. With the added amount of detail and flexibility also come many unknowns, and thus much time is required to understand all the complexities in the model.

The objective of the model simulation described in this section is to test[12] RAMS as a representative mesoscale model for wind flow over complex terrain with domain size 10 to 100 km. The experiment uses Sumanik Mountain, near Whitehorse as a test case. Sumanik has been monitored at three locations and the wind speed data will, in future work, be used to evaluate the results.

The ultimate desired outcome of this experiment is for RAMS to simulate wind flow over Sumanik Mountain with fine grid spacing. It is desirable to produced wind speeds at 20 to 50 m above the ground surface. This would require vertical grid spacing of $\Delta z = 20$ m or finer. Horizontal grid spacing should no more than about $\Delta x = \Delta y = 100$ m to reflect the relatively rugged terrain.

This section describes results of one RAMS simulation in the early experimental stage. It must be clarified that the experimental model is coarse and not necessarily realistic, or well understood. That is, it has not been clear what effects certain parameter settings were causing. An example of this is the lateral boundary condition where there is no obvious setting to allow constant inflow conditions. This situation would be convenient where it is desirable for the model to settle to a steady state wind flow. However, the results do show some plausible aspects.

The following sections summarise the settings for input into the model. Full details of the variable settings are listed in the file called RAMSIN, which is shown in Appendix D

4.1 Domain and Grid

The domain size in the horizontal is 24 by 24 grid points with uniform spacing of $\Delta x = \Delta y = 1000$m. The co-ordinate system is terrain following with a flat top boundary. There are 18 levels in the vertical with $\Delta z = 200$m at the bottom grid and stretching by 1.145 times per cell in the upward direction. With this stretching ratio the top is at a height of about 14.4km above the lowest surface.

The time step is 10 seconds. There is also a short time sub-step to handle the pressure gradient force and divergence equation terms. These are terms involving the propagation of sound waves and the short time sub-step is set to 10/6 seconds. RAMS is run for a six-hour simulation time

4.2 Equations and Discretisation

The conservation equations are fully elastic, non-hydrostatic, but with no Coriolis effect. The temporal differencing scheme is a hybrid mix of forward and leapfrog. The velocity

[12] RAMS installed on a Sparc Unix (bought in 1997) at the Northern Forestry Centre in Edmonton, who has generously provided the author assistance and computer time to carry out the experimentation.

and pressure components are updated using leapfrog, and all other prognostic variables use forward difference. Second order accuracy is used in the prognostic variables for both the leapfrog and the forward advective scheme. Horizontal pressure gradient is evaluated from an "appropriate" weighting between the vertical pressure gradient and the gradient along a sloping sigma-z surface. The horizontal and vertical diffusion coefficient are computed as the product of the 3-D rate-of-strain tensor and a length scale squared.

4.3 Boundary Conditions

In the lower boundary, the terrain elevation is read from a data file representing Sumanik Mountain. The elevation points are spaced at 100m. The land coverage is set to 100 % land. The surface roughness is 0.02 m (ZROUGH=0.02) for the whole model. The terrain grid points are flattened from the third point from the lateral boundary in each direction.

For surface layer and soil parameterisation there is no heat or moisture flux from ground to atmosphere. The cover of the surface layer is tundra. The average seasonal temperature is set to 263° Kelvin, which is used to determine the leaf area index and fractional coverage of vegetation (it should reflect vegetation with bare branches since it is a winter condition).

The minimum permitted horizontal velocity in the lowest model grid is 0.25 m/s. It is used as a minimum value in computing the friction velocity u_*. The reason for this parameter is to allow the sub-grid eddies to have a characteristic mean wind speed in variable direction causing the effective friction velocity to be positive.

The model top boundary is rigid with a five-level Rayleigh friction (i.e. $\frac{\partial \overline{w}}{\partial t} + ... = ... - \frac{\overline{w}}{\Im_0}$) absorbing layer and a dissipation time scale ($\Im_0$) of 60 seconds. This is a bogus additional damping term included in the top five model layers.

The lateral boundaries are set with the Klemp-Wilhelmson condition in which the normal velocity component specified at the boundary is effectively advected from the interior assuming a propagation speed of 10 m/s. This is intended to be similar to a dominant gravity wave phase speed. All variables other than the velocity component are set such that the lateral boundary value of each variable is set to the value in the field immediately adjacent to the boundary in the interior. This causes a zero-gradient condition; it is most commonly used.

4.4 Initial Conditions

Sounding data from the upper air data collected at the Whitehorse airport is used to initialise the atmospheric conditions in the model (see Table 2 below). The profile of horizontal wind speed has been modified to reflect a typical prevailing wind direction from the south-east. The first elevation of 500m is a dummy elevation set below the lowest ground level. It is meant to accommodate some (as yet impenetrable) problems with the RAMS model. The elevation 703m is the release height of the sounding balloon at the airport.

Height (m a.s.l.[13])	Pressure (mbar)	Temperature (C)	(%RH)	US (m/s)	VS (m/s)
500	938	10.7	54	0	0
703	916	9.4	54	0	0
1278	850	3.2	65	-4	4
2801	700	-6.5	63	-4	4
5290	500	-23.3	74	-3	3
6840	400	-33.3	52	-3	3
8700	300	-47.7	59	-3	3
9880	250	-56.9	56	-4	4
11340	200	-56.5	31	-4	5
13230	150	-52.7	9	-5	5
15890	100	-54.9	7	-5	5
18210	70	-52.7	6	-6	6
20380	50	-57.3	7	-6	6
23650	30	-58.5	7	-6	6
26220	20	-59.7	6	-6	6

Table 2 - Representative sounding data from Whitehorse airport. US is the easterly and VS is the northerly wind.

4.5 Microphysics

The moisture algorithms are activated to allow for advection, diffusion and surface flux. All water substance in the atmosphere is assumed to occur as vapour even if supersaturation occurs. Cloud, rain, pristine ice, and aggregates are activated. Rainfall velocity is artificially reduced to the stability limit. No short-wave or long-wave radiation or convective parameterisation are activated.

[13] a.s.l. – above sea level

4.6 Results and Discussions

The most recent simulation results showed a relatively stable model (meaning: no occurrence of wind speeds exceeding 20 m/s). The run time on the workstation was under half an hour for a six-hour simulation.

The last run was a significant improvement over the previous one, which had a smaller grid spacing of 500 m and would blow up in less than two hours of simulation time. In the previous run the time step was reduced down to 1 second, which considerably lengthened the run time but caused no significant improvement in stability. To stabilise the model many features such as damping and diffusion were modified. There seemed to be little improvement to the stability, the model would still crash, often before the second simulation hour. Upon checking the Courant number C_o for stability it was found that

$$C_o = \frac{\bar{u}\Delta t}{\Delta x} = \frac{8.5 \times 10}{500} = 0.17$$

which satisfies the conditions for stability $C_o < 1$. Thus it is not evident why the earlier simulations were unstable, but whatever the reason, increasing the grid spacing to 1000 m definitely improved the stability.

The results of the RAMS model run using the configuration described in this chapter are shown as vectors depicting the horizontal velocity[14] as seen in Figure 4 through Figure 6. The top of the model is North. The thicker 1000m and the 1500m contour lines represent the terrain elevation. The thinner lines are pressure contours.

Figure 4 shows the initial state defined by the wind speed profile in the sounding data. The velocity vectors all point towards the north-west. Referring back to the wind speed profile in Section 4.4 one could easily deduce that the length of the vectors in the model run at time zero-hour correlate with the elevation in the model.

[14] Note that the length of the wind vectors represent the magnitude of the wind speed. At the time that these results were produced there were no set methods to measure the magnitude. It is apparently possible to create contours of wind speed magnitudes, which would be more appropriate in terms of modelling for predictions of wind energy potential.

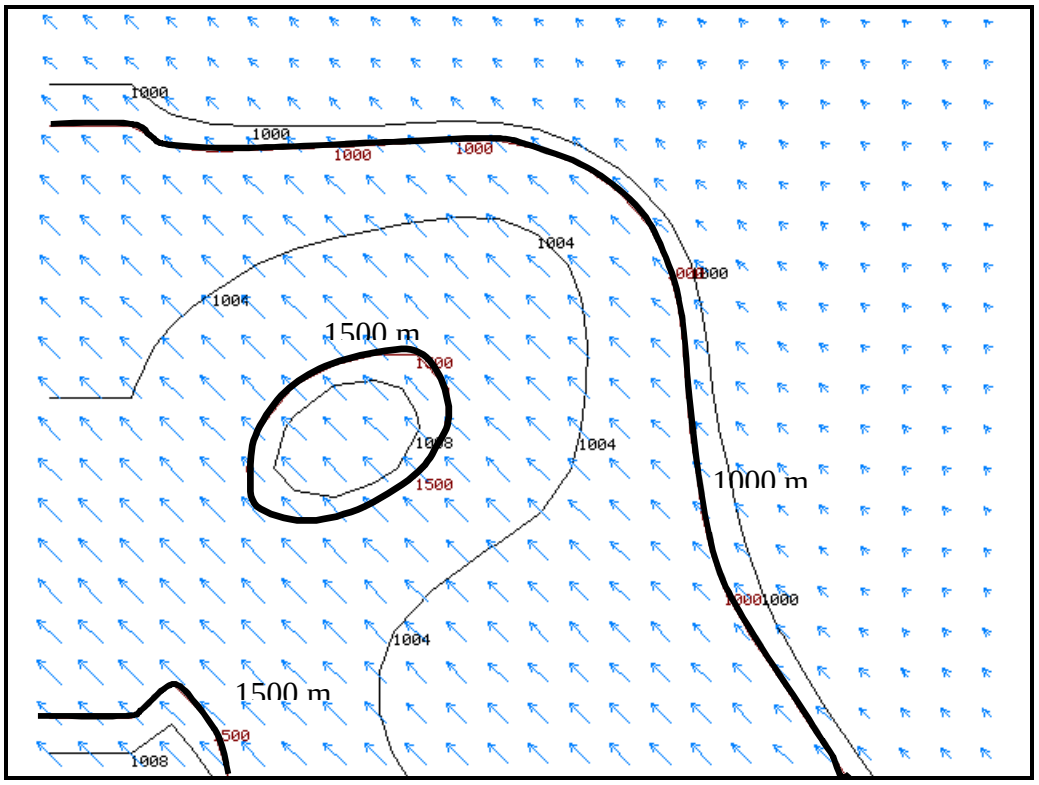

Figure 4 - Initialisation (time t = 00h). Thick contour is elevation, thin contour is pressure at ζ = 0. Arrows are horizontal velocity vectors.

In the second hour of the simulation (as shown in Figure 5) it can be seen that there is a wind speed-up (compare to Figure 4) over the top of the mountain. However, some of the air flows around the mountain as well. The near-zero wind flow in the lee (north-west) of the mountain is indicating a possible cavity or eddy zone as described in Figure 5 of Section 2.1.3.

The pressure contours are showing a drop in the atmospheric pressure everywhere in the domain, which doesn't correspond to the general negative (downward) vertical velocity[15] (except on the south-east flank of the hill marked by the dotted lines in Figure 5).

The wind directions at the inflow boundaries at the right and the bottom of the domain are not equal to those imposed at t = 0. It was not clear how to "fix" the inflow boundary conditions. The inflow seems to go in a northerly direction while, although there is no Coriolis force in effect, the outflow is rotated counter-clockwise towards a westerly direction in the north-west corner of the model.

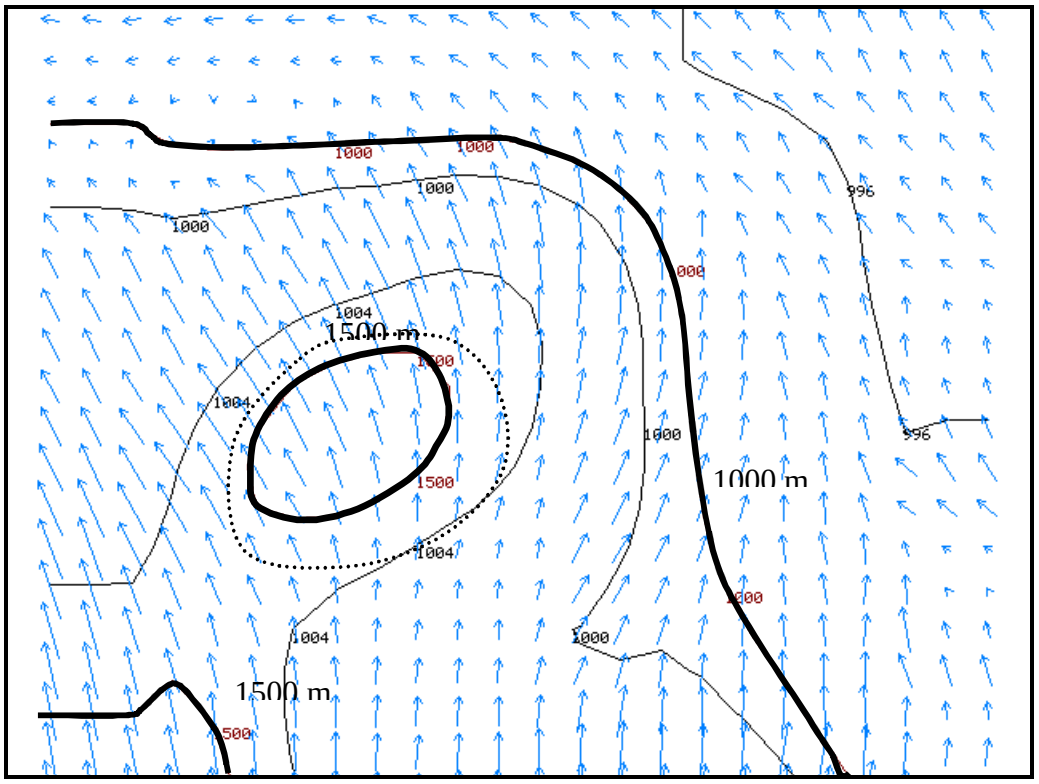

Figure 5 - Initialisation (time t = 02h). Thick contour is elevation, thin contour is pressure at ζ = 0. Arrows are horizontal velocity vectors.

[15] Referring to the vertical velocity contours in Figure 8 of Appendix E it can be seen that there is generally a negative vertical velocity in the model.

In the sixth hour as shown in Figure 6 it is clear that the inflow boundary conditions are not constant. The model has evolved to a state of chaotic motion where most wind activity now occur in the lower elevation within the domain. It can also be seen that the pressure has continued to drop.

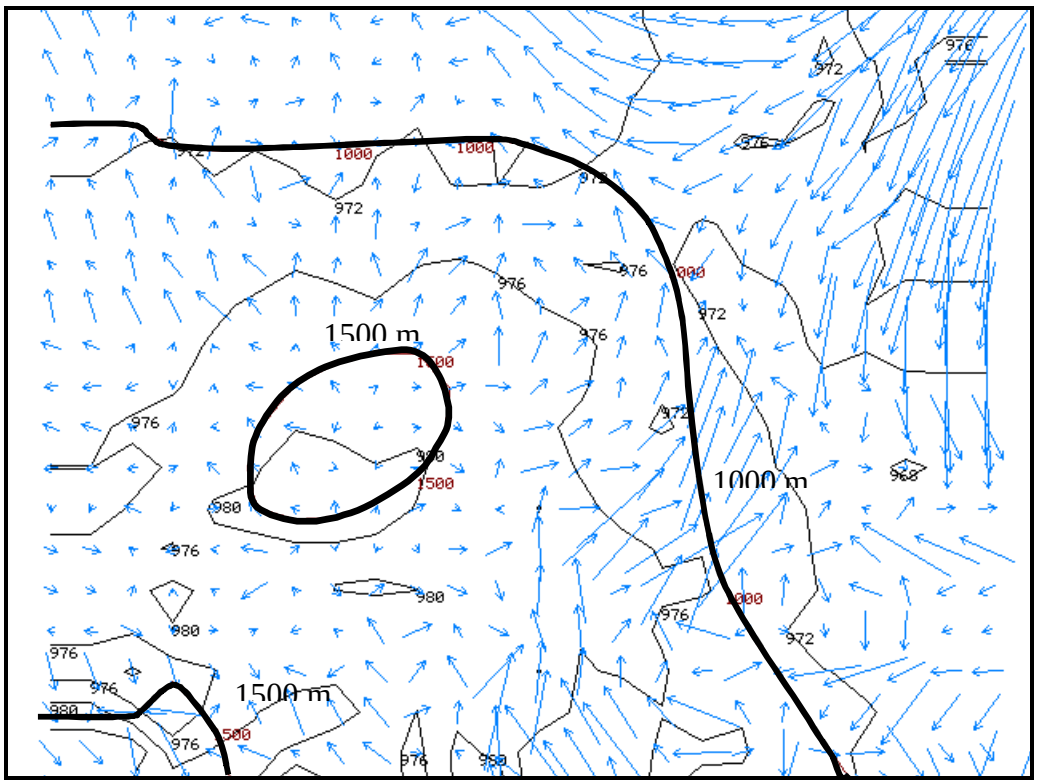

Figure 6 - Initialisation (time t = 06h). Thick contour is elevation, thin contour is pressure at ζ = 0. Arrows are horizontal velocity vectors.

The questions that arise from the last experimental simulation are as follows:

- ◇ Is the model losing mass?
- ◇ How is the Rayleigh friction layer affecting the model?
- ◇ Is the run time unrealistically long? If so then what is the optimal observation time?
- ◇ How can the inflow conditions be made constant?
- ◇ Will reducing the model grid spacing improve the simulation?
- ◇ Will reducing the time spacing improve the simulation?
- ◇ How strong is the buoyancy implied by positive w?

5 Conclusions

There are many existing software packages that will model wind flow over mountainous terrain. For predicting wind speed near the surface we could choose from several levels of complexity in simulation techniques. But, how sophisticated should a model be to satisfy result requirements is an issue that needs further study.

The comparison between microscale and mesoscale models is clear. Microscale models are steady state and are built for small domain sizes, i.e. less than 10 km, whereas mesoscale models are fully time-dependant and are for domains of the order 10 to 2000 km.

Mesoscale models are being seriously considered because of their high level of sophistication. They provide such features as grid nesting, high order closures, full set of conservation equations, etc. But there are issues that need to be understood when applying mesoscale models to wind flow over mountainous terrain of scale 10 to 100km. Can this domain scale be modelled with steady state conditions? Is Coriolis important? Can the models handle relatively steep terrain? How important are turbulent closure schemes? These are all relevant questions that will need to be answered through further literature search and further experimentation with the computer models.

In the RAMS model simulations performed to date it is not yet clear if this particular package is appropriate for modelling the present scale of interest. The lateral boundary conditions don't seem to provide constant inflow conditions. Finer grid spacing less than 1 km causes instability in the model and time step has to be increased to the point where the model runs are in the order of hours. However, it is still worthwhile to continue the model exercise until we can feel comfortable with the input parameters.

Other packages merit further investigation. The first ones on the list are ARPS and MSFD-PC. ARPS shows promise that reliable simulation results are possible. MSFD-PC is not as elaborate as the former but may satisfactorily produce the desired results. Further work is in order to test these models.

Acknowledgement

The experimental study of RAMS was facilitated by the support of the Northern Forestry Centre, in Edmonton, through their gracious offer of computer resources and personnel. The personnel to thank are Richard Carr, Peter Englefield, and Kerry Anderson. Other thanks go to John D. Wilson, U of Alberta, for editorial assistance and support for helping to clarify the theoretical aspects of atmospheric flows.

6 References:

Beljaars, A.C.M., Walmsley, J.L. and Taylor, P.A., 1987, "A mixed spectral finite difference model for neutrally stratified boundary layer flow over roughness changes and topography", Boundary-Layer Meteorol., 38:273-303.

Deaves, D.M., 1975, "Wind over hills: A numerical approach", J. Indust. Aerodyn. 1: 371-391.

Finnigan, J.J., 1988, "Air flow over complex terrain", Flow and Transport in the Natural Environment: Advances and Applications, CSIRO Division of Environmental Mechanics, Springer-Verlag, Berlin Heidelberg, 183-129.

Haugen, D.A., W.L. Kaimal, E.F. Bradley, 1971, "An experimental study of Reynolds stress and heat flux in the atmospheric boundary", Q. J. R. Meteorol. Soc., **97**, 168-180

Holton, J.R., 1992, " An Introduction to Dynamic Meteorology" Academic Press Limited, London.

Hunt, J. C. R., S. Leibovich and K. J. Richards, 1988, "Turbulent shear flow over hills", Quart. J. Roy. Meteor. Soc., **114**, 1435-1470.

Hunt, J.C.R., 1980, "Wind over hills", In Wyngaard, J.C. (ed.), Workshop on the Planetary boundary layer, Am. Meterol. Soc., Boston, pp 107-144.

Justus, C.G., 1978, "Winds and Wind System Performance", The Franklin Institute Press, Philadelphia, Pennsylvania.

Kaimal, J.C., J.C. Wyngaard, D.A. Haugen, O.R. Coté, Y. Izumi, S.J. Caughey, C.J. Readings, 1976, "Turbulence structure in the convective boubdary layer", J. Atmos. Sci., **33**, 2152-2169.

Kaimal, J.C., J.J. Finnigan, 1994, "Atmospheric Boundary Layer Flows: Their structure and measurement", Oxford University Press, New York.

Mason, P.J., and R.I. Sykes, 1979, "Flow over an Isolated Hill of Moderate Slope", Quart. J. R. Meteorol. Soc., **105**, 383-395.

Paulson, C.A., 1970, "The Mathematical Representation of Wind Speed and Temperature Profiles in the Unstable Atmospheric Surface Layer", J. Appl. Meteorolo. 9, 857-861

Pielke, R.A., 1984, "Mesoscale Meteorology Modelling", Academic Press, Inc., San Diego, CA, USA.

Stull, R.B., 1988, "An introduction to Boundary Layer Meteorology", Kluwer Academic Publishers, Dordrecht, The Netherlands.

Sykes, R.I., 1980, "An asymptotic theory of incompressible turbulent boundary-layer flow over a small hump", J. Fluid Mech.101: 647-670.

Tampeiri, F., 1987, "Separation features of boundary layer flow over valleys", Bound. Layer Meteor., **40**, 295-308.

Taylor, P.A., 1977a, “Some numerical studies of surface boundary-layer flow above gentle topography”, Boundary Layer Meteorol. 11: 439-465.

Taylor, P.A., 1977b, “Numerical studies of neutrally stratified planetary boundary-layer flow above gentle topography”, Boundary Layer Meteorol. 12: 37-60.

Taylor, P.A., J.L. Walmsley, and J.R. Salmon, 1983, “A simple model of neutrally stratified boundary-layer flow over real terrain incorporating wavenumber-dependent scaling”, Boundary-Layer Meteorology, **26**, 169-189.

Taylor, P.A., R.J. Lee, 1987, “Simple guidelines for estimating wind speed variations due to small scale topographic features”, Climatol. Bull. 18(2): 3-32.

Taylor, P.J. and Gent, P.R., 1974, “A model of atmospheric boundary layer flow above an isolated two dimensional ‘hill’; and example of flow above ‘gentle topography’” Boundary Layer Met., **7**, pp. 349-362.

Traci, R.M., G.T. Phillips and P.C. Patriaik, 1978 "Developing a site selection methodology for wind energy conversion systems" Science Applications Inc. for US Department of Energy, Report No. DOE/ET/20280-3.

Walmsley, J.L., J.R. Salmon, and P.A.Taylor, 1982, “On the Application of a Model of Boundary-Layer Flow Over Low Hills to Real Terrain”, Boundary-Layer Meteorol., **20**, 391-395.

Walmsley, J.L., P.A. Taylor, and R. Mok, 1980, “MS3DJH – A Computer Model for the Study of Neutrally Stratified Boundary-Layer Flow over Isolated Hill of Moderate Slope”, Rep. AQRB-80-008-L, Atmos. Environ. Service, Downsview, Ontario.

Walmsley, J.L., P.A. Taylor, and T. Keith, 1986, “A Simple Model of Neutrally Stratified Boundary-Layer Flow Over Complex Terrain with Surface Roughness Modulations (MS3DDJH/3R)”, Boundary-Layer Meteorol., **36**, 157-186.

Wyngaard, J.C., 1983, “Boundary-Layer Modelling”, In *Atmospheric Turbulence and Air Pollution Modelling* (F.T.M. Nieuwstadt and H. Van Dop, Eds.). Reidel, Hingham, MA, 69-106.

Wyngaard, J.C., 1988, “Convective processes in the lower atmosphere”, In *Flow and Transport in the Natural Environment: Advances and Applications* (W. Blumen, Ed.). CSIRO Division of Environmental Mechanics, Springer-Verlag, Berlin Heidelberg, 240-260.

Zemen, O., N.O. Jensen, 1987, “Modification of turbulence characteristics in flow over hills”, Q. J. R. Meteorol. Soc. 113: 55-80.

Appendix A – Historical Notes

The horizontally homogenous atmospheric surface layer was considered to be well understood by the 1970's (Finnigan, 1988). The Monin-Obukhov similarity theory has been confirmed by the Kansas and Minnesota boundary layer experiments (Haugen et al. 1971; Kaimal et al. 1976). Also during this period was the beginning of the application of the mixed layer scaling to the convective layer (Wyngaard, 1988).

Numerical models for flow over a hill were presented by Taylor and Gent (1974) and Deaves (1975). These models retained the full non-linear formulation with mixing length turbulence closure. In 1977 Taylor extended his computations for more complex, realistic terrain input and to cope with scales over which Geostrophic forcing and the Ekman boundary layer had to be considered (Taylor 1977a, b).

A very different approach was taken by Jackson and Hunt (1975; hereafter JH75), who introduced assumptions (notably linearisation) that allowed them to give an analytical solution. Their two-layer model comprised an inviscid outer layer and an inner surface layer in which turbulent stress divergence affects the momentum balance. This model was linearised, which restricted it to low hills. The fact that it was analytic allowed it to be easily applied to a variety of terrain and its predictions could serve as guidelines to estimate mean velocities in many different circumstances (Hunt 1980; Taylor and Lee 1987).

As more field data became available a series of developments were made in attempt to remove some of the restrictions of the original JH75 model. Mason and Sykes (1979) produced a 3-D version. Sykes (1980) published some careful analysis that cautioned of internal inconsistencies in the basic formulation. In 1980 Walmsley et al. developed the computer code for the first of the series of MS3DJH (**M**ason and **S**ykes **3 D**imensional **J**ackson and **H**unt) numerical models.

Walmsley et al. (1982) simulated flow over real terrain using MS3DJH. They encountered reasonable success in matching predictions with field and wind tunnel data. The model went through a number of changes to become MS3DJH/3R (Walmsley et al., 1986; Beljaars et al. (1987)). These new changes coped with simultaneous changes in roughness and elevation. The requirements this imposed for a more sophisticated turbulence closure have pushed model computations back into the numerical domain. The model at this stage incorporates wave-number-dependent scaling (Taylor et al., 1983), efficient Bessel function table look-ups, and wind speed modifications due to surface roughness variations.

As can be seen above, the linear theory is advantageous in that it can derive formulae for flow analytically for a wide range of conditions. What it cannot do is describe large perturbations to the flow. To describe hill flows with large slopes (large changes in speed) or to provide a deeper description of turbulence, one must accommodate non-linear and a more realistic closure then the mixing length of JH75. This leads back to numerical modelling.

Perhaps the most advanced non-linear numerical model for hill flow on the microscale so far is the mixed-spectral finite-difference (MSFD) model, which was first released in April

1993. It was developed to integrate mixing length, E-epsilon, and E-epsilon-tau turbulence closure options into a single model. MSFD is primarily a research model; MS-Micro/3 is an applications model. The higher-order turbulence closure options, however, provide information on turbulence and turbulent kinetic energy that is not available in MS-Micro/3.

Appendix B – Mesoscale Models

The following table compares the mesoscale models by their capabilities. It is not yet complete, as it is part of a larger research chapter for future work. The purpose of this table is to provide a summary on recent mesoscale developments.

Feature	**ARPS**	**MC2 – RPN**	**MM5**	**RAMS**	**RSM/MSM**	**COAMPS**
Full name	Advanced Regional Prediction System	Mesoscale Compressible Community. Physics package by Recherche en Prévision Numèrique (RPN)	Fifth-Generation Penn State/NCAR Mesoscale Model	Regional Atmospheric Modelling System	Regional Spectral Model (hydrostatic)/ Meso-scale Spectral Model (non-hydrostatic)	The Coupled Ocean/Atmosphere Mesoscale Prediction System
Founders	Too many contributors to name	Robert and Yakimiw (1986)	Anthes and Warner (1978)	R.A. Pielke and W.R. Cotton (1986)		
Institution of Origin	U of Oklahoma	RPN, Env. Canada &(UQAM)	Penn State /NCAR	Colorado State University	NCEP (National Centers for Env. Prediction)	Naval Research Lab., Marine Met. Division
Portability, Operating System	Unix, Linux, NT		Unix, Linux (pre-proc. prog. not tested), 128 Mb RAM & 2 Gb HD	Unix, Linux, NT	Unix Cray, SGI, HP, Sun SPARC, IBM RISC including SP2, and DEC Alpha	Unix, Cray, SGI, DEC ALPHA, SUN and HP workstations
Cost	Free	$$	Free	>$8000US to register and >$2000us/yr	Free	Free, w/ memorandum of agreement
Support	User group, email support	One full-time personnel, courses	User group, courses, one full-time personnel	Yes, user group and individual support	Not clear, online instruction for installation.	
Web site	Yes	None dedicated to MC2	Yes, well developed	Yes, one dedicated, two less elaborate.	Yes, limited documentation	Yes, with documentation

Feature	**ARPS**	**MC2 – RPN**	**MM5**	**RAMS**	**RSM/MSM**	**COAMPS**
Online manuals	From the website itself	No	From the website, very extensive	Yes, ASTER Division and NOAA website	Yes, limited	
Equations	Non-hydrostatic, compressible primitive equations	Non-hydrostatic, compressible	Non-hydro. & hydro, compressible	non-hydrostatic, quasi-compressible	Non-hydro. & hydro, compressible	Non-hydrostatic, compressible equations
Scale/Resolution:	$0.1 < \Delta x < 15$km microscale, stormscale, mesoscale.		Global 30 sec	From planetary hemisphere to Flow around buildings (2 km to 2000 km)		
Grid Structure	Arakawa C-grid. Terrain following, equal x,y spacing, stretching in vertical	Arakawa C-grid for hor., Tokioka B-grid for vert.	B-grid staggering of hor. Velocity, vertical vel. is staggered vertically. Terrain following	terrain-following, pressure-type surfaces, polar stereographic, Cartesian, stretching		Sigma-z vertical coordinate
Spatial discretisation	2^{nd} and 4^{th} order quad. Conserved FD for advect., 2^{nd} order for other terms.		Second Order Centered	Arakawa-C staggered grid for thermodynamic and momentum variables to reduce finite differencing error. Forward-backward time-split second-order finite time and space	spectral model	Arakawa-Schubert scheme A for analysis grid conventions, Arakawa-Schubert Scheme C for model grid conventions

Feature	**ARPS**	**MC2 – RPN**	**MM5**	**RAMS**	**RSM/MSM**	**COAMPS**
				differencing		
Temporal discretisation	Large T steps: 2nd leap-frog scheme (with Asselin time filter option). Small T steps: 1st order for/back explicit w/ 2nd cent. implicit	Semi-Implicit, Semi-Lagrangian time scheme	Leap-frog steps w/ Asselin filter.	Forward, leap-frog , or leap-frog in vel. & press. and forward in other vars		
Sub-grid scale turbulence parameterisation	Smargorinsky-Lilly diag. 1st O, 1.5-O tke formulation, Germano dynamic closure, isot. & anisot. Turb. treatment			1st O Smagorinsky-type vertical eddy viscosity mixing with a Richardson number		Level 2.5 TKE closure
Lateral BC's	Options: periodic, rigid, zero-grad, wave rad., externally forced, & user specified, const. inflow/ outflow cond'n,			zero-grad., radiative outflow cond'n, nudging scheme, ave. velocity scheme., periodic		Time-dependent BC's: Davis (QJRMS 1976), Perkey-Krietzberg (MWR 1976), Periodic, radiation, or fixed
Top & bottom BC's	Options: rigid, zero-grad., periodic, & top rad. Cond'n using			Top: w=0, gravity wave cond'n, Raleigh friction absorbing		

Feature	**ARPS**	**MC2 – RPN**	**MM5**	**RAMS**	**RSM/MSM**	**COAMPS**
	Rayleigh sponge layer			Bot.: roughness, moisture, radiation		
Initial State	HH using single sounding, analytic functions, or 3D HH data.	Sounding????	Multiple sounding, surface reports, incl. wind, temp., RH, sea-level pressure and surf. temp.	Multiple soundings or HH single sounding	Sounding ???	Sounding ???
Coriolis	Yes		Yes	Yes		
Physics	Yes, for acoustic oscillations	PBL based on tke, impl. vert. Diffu., SSL based on ST, surf. Temp. pred., rad. Scheme in cloud, shallow conv., Kuo-type deep conv., grid-scale cond.		modified Kuo	-Radiation -PBL and surface -Precipitation and diffusion -Gravity wave drag	-sub-grid scale mixing -cumulus parameterisation -radiation -explicit moist physics

Notes: O – order, tke – turbulent kinetic energy, RH – relative humidity, PBL – Planetary Boundary Layer, SSL – Stratified Surface Layer, ST – Similarity Theory

Appendix C – Web Sites

The following is a list of web sites, which provide information on the known existing mesoscale models.

RAMS

Documentation relating to the applications of the regional atmospheric modeling system (rams) at the NOAA air resources laboratory are found here
http://www.arl.noaa.gov/data/models/rams/usrgde.html

Mission Research Centre, ASTER Division. Well developed site with a good technical document and downloads for registered users.
http://www.aster.com/index.shtml

MM5

This is the official MM5 mesoscale model home page run by the Pennsylvania State University and National Centre for Atmospheric Research (PSU/NCAR).
http://www.mmm.ucar.edu:/mm5/mm5-home.html
This site is well documented and provides all the software in the PSU/NCAR mesoscale modelling system, which is dedicated to the public domain.

MC2

Real-time high-resolution weather forecasting during MAP (Mesoscale Alpine Programme) using the non-hydrostatic MC2 model
http://mocsh26.map.uibk.ac.at/mc2/

The University of British Columbia Weather Forecast Team
http://spirit.geog.ubc.ca/wxfcst/

Canadian Meteorological and Oceanographic Society Web site, which contains abstracts to, papers related to the MC2 model. These papers cover the people, development, and applications using MC2.
http://www.meds-sdmm.dfo-mpo.gc.ca/cmos/abstre.html

ARPS

The home page to the Advanced Regional Prediction (ARPS). It is a comprehensive web site containing a multitude of pages such as: What's New, Model Overview, Current Version, Future Plan, Documentation, User Support, FAQ, User's Info, Research Applications, Realtime Applications, Realtime, Forecast at CAPS, Download, Meet the People, Feedback, and the Developers' Corner
http://www.caps.ou.edu/ARPS/

RSM

The NCEP Regional Spectral Model (RSM) Home Page. This site has documentation, plans, operational and experimental results, publications, and collaborations.
http://sgi62.wwb.noaa.gov:8080/rsm/rsm.html

COAMPS

This is the Naval Research Laboratory Marine Meteorology Division wed site. It provides information such as the programme overview, tutorial, documentation, daily forecasts, publications, download changes, and what's new.
http://www.nrlmry.navy.mil/~coamps/

Appendix D – RAMS Input Parameters

The following is the name list showing the values used to run the last RAMS model run

```
$MODEL_GRIDS
  EXPNME  = 'Yukon Grid',
  IOTYPE   = 0,
  RUNTYPE = 'INITIAL',
  TIMEUNIT = 'h',
  TIMMAX = 6, ! It is run for 6 hour simulation time
  NGRIDS = 1, ! There is only one grid with no nested grids
  NNXP    =  24,34,74, ! The grid is three-dimensional. It is 24 by 24 in the horizontal
  NNYP    =  24,34,74,
  NNZP    =  25,30,30, ! and 25 levels in the vertical
  NNZG    =  1,7,7, !# of soil gridpoints There is one soil level.
  NXTNEST =  1, 1, 2, 3, ! # of the next coarser grid
  IHTRAN  =      1,  ! The grid is set in a polar stereo-graphic co-ordinate system
  DELTAX  =  1000., ! The spacing is 1000m by 1000m in the horizontal
  DELTAY  =  1000.,
  DELTAZ  =    200., ! 200m in the vertical with a stretching ratio
  DZRAT   =    1.145, ! of 1.145 per cell in the upward direction
  DZMAX   =    2000., ! The option for maximum vertical grid spacing of 2000m limits the grid size to
                                about the 18th level at a height of 14.4km above the surface.
  ZZ=0., 25., 75., 150., 250., 500., 750., 1000., 1500., !1
     2000., 2500., 3250., 4000., 5000., 6000.,  ! This option is not used
  DTLONG  =   10., ! The time step is 10 seconds
  NRATIO  =   6, ! This is a short time step ratio to handle the pressure gradient force and divergence
                        equation terms.
  IMONTH1 = 10, ! date related for prognostic real time modelling
  IDATE1 = 6,
  IYEAR1 = 99,
  STRTIM = 00,
  NSTRATX =   1, 4,3,
  NSTRATY =   1, 4,3,
  NNDTRAT =   1, 3,3,
  NESTZ = 0,
  NSTRATZ=4,4,3,3,3,3,2,2,2,2,1,1,1,1,
  POLELAT   =    60.7333, !  Latitude of pole point
  POLELON  =   -135.25, !  Longitude of pole point
  CENTLAT=    60.7333, 61.0,61.0,
  CENTLON=  -135.25, -135.0,-135.0,
  NINEST  =   1, 0, 0,
  NJNEST  =   1, 0, 0,
  NKNEST  =   1, 1, 1,
  NNSTTOP =   1, 1, 1, !  no: 0  yes: 1  if  grid goes to
  NNSTBOT =   1, 1, 1, !  top/bottom of the coarsest grid
  GRIDU   =  0., 0., 0., !  u & v component for moving
  GRIDV   =  0., 0., 0., !  grids (NOT WORKING in 3a)
 $END
 $MODEL_FILE_INFO
  TIMSTR = 18,
  HFILIN = 'yk.h18h',
```

```
 IOUTPUT=       1,  ! no files:0 save/dispose:1
 HFILOUT='yukh',   !  History file prefix
 AFILOUT='yuka',   !  Analysis file prefix
 HFUNITS='h', AFUNITS='h', ! Hist/anal units (M,m,H,h,S,s)
 FRQHIS  =10800.,   FRQANL  = 10800.,
 INITIAL =   1,
 VTIME = 0,12,24,
 VARFIL = 'iv01-oct-99-00','iv01-oct-99-12','iv01-oct-99-12',
 IVWIND =       0,
 NUDLAT   =     2,
 TNUDLAT = 10800, ! nudging
 TNUDCENT = 21600,
 TNUDTOP = 1800,
 ZNUDTOP  =     17000.,
 FRQPRT  =   3600.,
 FRQIPR  =   10800., !  Integral print frequency
 FRQIST  =   10800., !  Integral store frequency
 ISTPFL  =       1, !  Timestep msg frequency flag
 INITFLD =       1, !  Init. field prn flag 0=no 1=yes
 INPRTFL =       1, !  Namelist print flag  0=no  1=yes
 SFCFILES = 'msfc',  !  Surface files path and prefix
 ITOPTFLG = 1,1,0,1,2, ! read terrain elevation from data file
 IPCTLFLG = 2,1,0,1,2, ! Interpolate from lon/lat dataset: 1
 ISSTFLG  = 2,0,0,0,0, !  Fill data in 'ruser3a.f': 2
 IVEGTFLG = 2,1,0,1,1,
 ITOPTFN = './1H', './2H', './3H', './4H',
 IPCTLFN = './1L', './2L', './3L', './4L',
 ISSTFN  = './S',
 IVEGTFN = './1V', './2V', './3V', './4V',
 SILAVWT  = 1., 1., 1.,0.,
 TOPTWVL  = 9., 4., 4.,4.,
 PCTLWVL  = 4., 4., 4.,4.,
 SSTWVL   = 4., 4., 4.,4.,
 MKCOLTAB = 0,
 COLTABFN = '/data/smoke/rams3b/data/micro/ct2.0',
 EVPTABFN = '/data/smoke/rams3b/data/micro/et2.0',
$END
$MODEL_OPTIONS
 NADDSC   =    0,0,0,0,
 NTOPSMTH =       0,
 IZFLAT  =       2, ! elevation grid points are flattened
 ITMDIFF =       3, ! temporal differencing is a hybrid of forward and leap-frog. The velocity and
                       pressure components are updated using leap-frog, and all other prognostic
                       variables use forward difference.
 NONHYD  =       1, model is non-hydrostatic with a fully elastic continuity equation.
 SSPCT   =     0.33, ! Effective speed of sound
 IMPL    =      1, ! propogation of sound waves in vertical are calculated implicitly
 ICNTEQ  =      2,
 WTKD    =     1.,
 ICORFLG =      0, ! no Coriolis effects
 IBCTOP  =      0, ! top boundary condition is rigid
 IBND    =      1, ! lateral boundary condition
 JBND    =      1,
 CPHAS   =     10.,
```

```
 LSFLG  =      0,
 NFPT   =     5,
 DISTIM =     60.,
 TIMSCL =     0., ! no velocity spin up during model initialisation
 KSPIN  =     7,
 KMSPIN =     25,
 IPRSPLT =    0,
 IADVL  =     2,
 IADVF  =     2,
 IPGRAD =     1,
 FILT4  =    000.,
 FXLONG =   0.0000,
 FYLONG =   0.0000,
 ISWRTYP =   0, ! Radiation parameters
 ILWRTYP =   0,
 RADFRQ  = 900.,
 LONRAD =   0,
 NNQPARM =  0,1,1,0, ! Cumulus parameterization parameters
 CONFRQ  = 1200.,
 WCLDBS  =  -0.05,
 ISFCL   = 0, ! Surface layer and soil parameterization
 NVGCON =     9,
 TSEASN =   263.,
 TVGOFF =    0.,
 VWTRCON =    .000,
 UBMIN  =   0.25,
 PCTLCON =  1.0,
 NSLCON =   12,
 ZROUGH =  0.02, ! ground roughness z0
 ALBEDO =   0.,
 SEATMP  = 277.,
 DTHCON  =  0.,
 DRTCON  =  0.,
 SOILDZ  =  0.,
!  SLZ   = -.4, -.25, -.125, -.05, -.025, -.01,  0.,
 SLZ = -.025,-.01,0.,
!  SLMSTR =  0.65, 0.6, 0.6, 0.5, 0.5, 0.4, 0.4,
 SLMSTR = .5,.4,.4,
!  STGOFF = -5.,-2.,.5,1.5,3.,5.,7.,
 STGOFF = 3.,1.,0.,
 IDIFFK = 3,2,2,3,1,
 CSX = .20,.20,.20,.20,.20,
 CSZ = .20,.20,.20,.20,.20,
 XKHKM = 1.,3.,3.,3.,3.,
 ZKHKM = 1.,3.,3.,3.,3.,
 AKMIN= 2.,1.,2.,2.0,1.,
 NLEVEL  =  1, 2, 3,3,1, ! Microphysics
 INUCPRG =  0, 0, 0,0,0,
 ICLOUD =   1, 1, 1,0,0,
 IRAIN  =   1, 1, 1,0,0,
 IPRIS  =   1, 1, 0,0,0,
 ISNOW  =   0, 0, 0,0,0,
 IAGGR  =   1, 1, 1,0,0,
 IGRAUP =   0, 0, 0,0,0,
```

```
  IHAIL  =   0, 0, 0,0,0,
  CPARM  =  .3e9,  .3e9, 0., 0., 0.,
  RPARM  = .1e-2, .1e-2, 0., 0., 0.,
  PPARM  =    0.,    0., 0., 0., 0.,
  SPARM  = .1e-2, .1e-2, 0., 0., 0.,
  APARM  = .1e-2, .1e-2, 0., 0., 0.,
  GPARM  = .1e-2, .1e-2, 0., 0., 0.,
  HPARM  = .3e-2, .3e-2, 0., 0., 0.,
  AMI0   =  1.e-12,
  GNU =      1.,   1.,  1.,  1.,  1.,   1.,  1.,  ! gamma shape parameters
$END
$MODEL_SOUND
!     Flags  for single sounding initialization:
  IPSFLG=0,  ! PS array contents: 0=P (mb) 1=z (m) 2=Psfc (mb)
  ITSFLG=0,  ! TS array contents: 0=T (C)  1=T (K) 2=pot T (K)
  IRTSFLG=3, ! RTS array content: 0=Td (C) 1=Td (K) 2=r (g/kg)
           !                    3=RH (%) 4=T-Td (K)
  IUSFLG=0,  ! US; VS array contents:  0=u,v components (m/s)
           !                    1=umoms (dir)  vmoms (speed)
  IUSRC = 0, ! Source of wind profile: 0=umoms,vmoms valid at
           !     soundings levels  (PS)
           !                       -1=usndg,vsndg valid at
           !     model levels  (Z)
  HS = 500., 703., 1278., 2801., 5290., 6840., 8700., 9880.,
      11340.,13230.,15890.,18210.,20380.,23650.,26220.,
  PS = 938., 916., 850.,  700.,500., 400., 300., 250., 200.,
      150.,  100.,70.,50.,30.,20.,
  TS = 10.7, 9.4, 3.2,-6.5,-23.3,-33.3,-47.7,-56.9,-56.5,
     -52.7,-54.9,-52.7,-57.3,-58.5,-59.7,
  RTS =54.,54.,65.,63.,74.,52.,59.,56.,31.,9.,7.,6.,7.,7.,6.,
!   US = 0., 0.,150.,215.,200.,195.,195.,205.,215.,270.,220.,255.,270.,275.,285.,
!   VS = 0., 0.,15.4,15.4,13.4,22.6,24.2,20.1,20.1,13.4,8.2,7.7,10.3,15.4,11.3,
  US = 0., 0., -4., -4., -3., -3., -3., -4., -4., -5., -5.,
     -6., -6., -6., -6.,
  VS = 0., 0.,  4.,  4.,  3.,  3.,  3.,  4., 5.,  5.,  5.,
      6.,  6.,  6.,  6.,
  USNDG = 0.,
  VSNDG = 0.,
  KMEAN1 = 0,
  KMEAN2 = 0,
  UMEAN = 0.0,
  VMEAN = 0.0,
 $END
 $MODEL_PRINT
  NPLT  =  3,
  IPLFLD = 'UP', 'VP', 'WP',
  PLFMT = '0PF7.2','0PF7.2','0PF7.2',
  IXSCTN = 3,3,3,
  ISBVAL = 1,1,1,
 $END
C     'UP'    - UP(M/S)     'RC'   - RC(G/KG)    'PCPT' - TOTPRE
C     'VP'    - VP(M/S)     'RR'   - RR(G/KG)    'TKE'  - TKE
C     'WP'    - WP(CM/S)    'RP'   - RP(G/KG)    'HSCL' - HL(M)
C     'PP'   - PRS(MB)     'RA'   - RA(G/KG)    'VSCL' - VL(M)
```

```
C     'THP'  - THP(K)
C     'THETA'- THETA(K)    'RL'   - RL(G/KG)    'TG'   - TG (K)
C     'THVP' - THV'(K)     'RI'   - RI(G/KG)    'SLM'  - SLM (PCT)
C     'TV'   - TV(K)       'RCOND'- RD(G/KG)    'CONPR'- CON RATE
C     'RT'   - RT(G/KG)    'CP'   - NPRIS       'CONP' - CON PCP
C     'RV'   - RV(G/KG)    'RTP'  - RT'(G/KG)   'CONH' - CON HEAT
C                                   'CONM' - CON MOIS
C     'THIL' - Theta-il (K)   'TEMP' - temperature (K)
C     'TVP'  - Tv' (K)        'THV'  - Theta-v     (K)
C     'RELHUM'-relative humidity (%)        'SPEED'- wind speed (m/s)
C     'FTHRD'- radiative flux convergence (??)
C     'MICRO'- GASPRC
C     'Z0'   - Z0 (M)      'ZI'   - ZI (M)      'ZMAT' - ZMAT (M)
C     'USTARL'-USTARL(M/S) 'USTARW'-USTARW(M/S) 'TSTARL'-TSTARL (K)
C     'TSTARW'-TSTARW(K)   'RSTARL'-RSTARL(G/G) 'RSTARW'-RSTARW(G/G)
C     'UW'   - UW  (M*M/S*S)                    'VW'   - VW (M*M/S*S)
C     'WFZ'  - WFZ (M*M/S*S)                    'TFZ'  - TFZ (K*M/S)
C     'QFZ'  - QFZ (G*M/G*S)                    'RLONG'- RLONG
C     'RSHORT'-RSHORT
 $ISAN_CONTROL
   MSTAGE = 0, 1, 1,
   NATIMES = 1,
   IAHOUR = 12,
   IADATE = 15,
   IAMONTH = 10,
   IAYEAR = 98,
   IAPR = '/data/fire3/rams3b/yuokn/gribll',
   IARAWI = '/data/fire3/rams3b/yukon/mandua.1999100112',
   IASRFCE = '/data/fire5/dbms/rams_sfcin',
   IFNPRS = 'ip',
   IOFLGP= 1,
   IFNISN = 'ii',
   IOFLGI= 1,
   IFNSIG = 'is',
   IOFLGS= 1,
   IFNVAR = 'iv',
   IOFLGV= 1,
 $END
 $ISAN_PRESSURE
    NPRX=137,
    NPRY=46,
    NPRZ=5,
    WPLON =  -168.0,
    SPLAT =   33.0,
    SPCNPRX = 1.0,
    SPCNPRY = 1.0,
    LEVPR  = 1000,850,700,500,250,
 $END
 $ISAN_ISENTROPIC
    NISN = 45,
    LEVTH =  232,233,234,235,236,237,238,240,242,244,246,248,
     250,252,254,257,260,263,266,269,272,276,280,284,288,293,
     298,304,310,317,325,334,345,360,375,395,415,435,460,485,
     525,575,635,700,785,
```

```
  NIGRIDS = 1,
   TOPSIGZ =  9000.,
   HYBBOT  =  6000.,
   HYBTOP  =  7000.,
   SFCINF  =  1000.,
   SIGZWT  =  1.,
   NFEEDVAR = 1,
   MAXSTA=    2,
   MAXSFC=    2,
   NONLYS  =      1,
!    IDONLYS ='76458',
IDONLYS = 'ADQ','FAI','CDB','ANC','YAK','ANN','YXY','YVQ','YYE','YXS',
   'YZT','YBK','YZS','YCB','YUX','YVN','WPH','YAH','WZC','YVP','YYR',
   'YPL','YYQ','YQD','YXE','YSM','WSE','WLW','UIL','SLE','MFR','GEG',
   'BOI','SLC','GGW','BIS','RAP','LND','LBF','INL','STC','GRB','Y62',
   'PIA','PIT','BUF','YWA','WMW','ALB','CAR','YZV','WQI','YJT','YYT',
   'WSA','CHH','WAL','IAD','DAY','PAH','TOP','UMN','DDC','DEN','GJT',
   'ELY','DRA','OAK','TFX','YEV','WZB','WLO',
   NOTSTA  =      0,
   NOTID   ='r76458',
   STASEP  =     .25,
   ISTAPLT =      0,
   ISTAREP =      0,
   IUPPER  =      1,
  IGRIDFL = 0,
   GRIDWT  =      .01, .01, .01,
   GOBSEP  =    2.0,
   GOBRAD  =    4.0,
  WVLNTH = 3000.,3000.,
  SWVLNTH = 3000.,3000.,
   RESPON  =    .80, .8,
 $END
 $ISAN_GRAPH
        ! Main switches for plotting
  IPLTPRS  =   0,     ! Pressure coordinate horizontal plots
  IPLTISN  =   0,     ! Isentropic coordinate horizontal plots
  IPLTSIG  =   0,     ! Sigma-z coordinate horizontal plots
  IPLTSTA  =   0,     ! Isentropic coordinate "station" plots

        !--------------------------------------
        ! Pressure plotting information
        !--------------------------------------
  ILFT1I  =   0,     ! Left boundary window
  IRGT1I  =  18,     ! Right boundary window
  IBOT1J  =   3,     ! Bottom boundary window
  ITOP1J  =  13,     ! Top boundary window
                !    Window defaults to entire domain if one equals 0.
  NPLEV   =   1,              ! Number of pressure levels to plot
  IPLEV   = 900,         ! Levels to be plotted
  NFLDU1  =   4,              ! Number of fields to be plotted
  IFLDU1  =   'U','THETA','GEO','RELHUM',        ! Field names
  CONU1   = 0.,0.,0.,0.,      ! Field contour increment
  IVELU1  = 2,0,0,0,          ! Velocity vector flag
```

```
      !---------------------------------------
      ! Isentropic plotting information
      !---------------------------------------
 ILFT3I  =  0,    ! Left boundary window
 IRGT3I  =  18,   ! Right boundary window
 IBOT3J  =  3,    ! Bottom boundary window
 ITOP3J  =  13,   ! Top boundary window
            !   Window defaults to entire domain if one equals 0.
            ! Upper air plots:
 IUP3BEG = 320,   ! Starting isentropic level for plotting
 IUP3END = 380,   ! Ending isentropic level
 IUP3INC =  60,   ! Level increment
 NFLDU3  =  5,          ! Number of fields to be plotted
 IFLDU3  =  'U','V','PRESS','GEO','RELHUM',      ! Field names
 CONU3   = 0.,0.,       ! Field contour increment
 IVELU3  = 1,0,         ! Velocity vector flag

      !---------------------------------------
      ! Surface plotting information
      !---------------------------------------
! Uses isentropic plotting window info

 NFLDS3  =  5,          ! Number of surface fields to plot
 IFLDS3  =  'U','V','PRESS','GEO','RELHUM',      ! Field names
 CONS3   = 0.,0.,0.,0.,0.,   ! Field contour increment
 IVELS3  = 1,0,0,0,0,        ! Velocity vector flag

      !---------------------------------------
      ! Sigma-z plotting information
      !---------------------------------------
! Uses isentropic plotting window info
 ISZBEG = 2,    ! Starting sigma-z level for plotting
 ISZEND = 8,    ! Ending sigma-z level
 ISZINC = 6,    ! Level increment
 NFLDSZ  =  5,          ! Number of fields to be plotted
 IFLDSZ  =  'U','V','PRESS','THETA','RELHUM',      ! Field names
 CONSZ   = 0.,0.,       ! Field contour increment
 IVELSZ  = 1,0,         ! Velocity vector flag

      !---------------------------------------
      ! "Station" plotting information
      !---------------------------------------
 NPLTRAW = 0,          ! Approximate number of raw rawinsonde plots per
                       !   frame. 0 turns off plotting.

 NSTIS3  =  2,         ! number of station surface plots
 ISTIS3  =  'PRESS','RELHUM','MIXRAT',    ! field names

      !---------------------------------------
      ! Cross-section plotting information
      !---------------------------------------
 NCROSS3 =    0,          ! number of cross section slabs
 ICRTYP3 =   2,1,         ! type of slab: 1=E-W, 2=N-S
```

```
 ICRA3   =   1,1,            ! left window
 ICRB3   =   35,43,          ! right window
 ICRL3   =   22,25,          ! cross section location
 NCRFLD3 =   3,              ! number of plots on each cross section
 ICRFLD3 =  'MIXRAT','RELHUM','THETAE',    ! field names
 THCON3  =   5.,5.,5.,       ! contour interval of isentropes
 ACON3   =   0.,0.,0.,       ! contour interval of other field
$END
!-------------------------------------
!   Field values for graphical stage
!-------------------------------------
!
!    Pressure       Isentropic    Station       Sigma-z
!-----------------------------------------------------------------------------
!    U              U             U             U
!    V              V             V             V
!    TEMP           PRESS         PRESS         PRESS
!    GEO            GEO           TEMP          THETA
!    RELHUM         RELHUM        RELHUM        RELHUM
!    MIXRAT         MIXRAT        MIXRAT
!    THETA          THETA
!    SPEED          SPEED
!    ENERGY         ENERGY
!    THETAE         THETAE
!    SPRESS         SPRESS
!
```

Appendix E Contour plots of the Sumanik Mountain RAMS Simulation

Figure 7 is a more detailed elevation contour of the Sumanik Mountain model. The top of Sumanik is located just left of centre. The top contour line is ~1500 m above sea level. The prevailing wind direction is from the south-east.

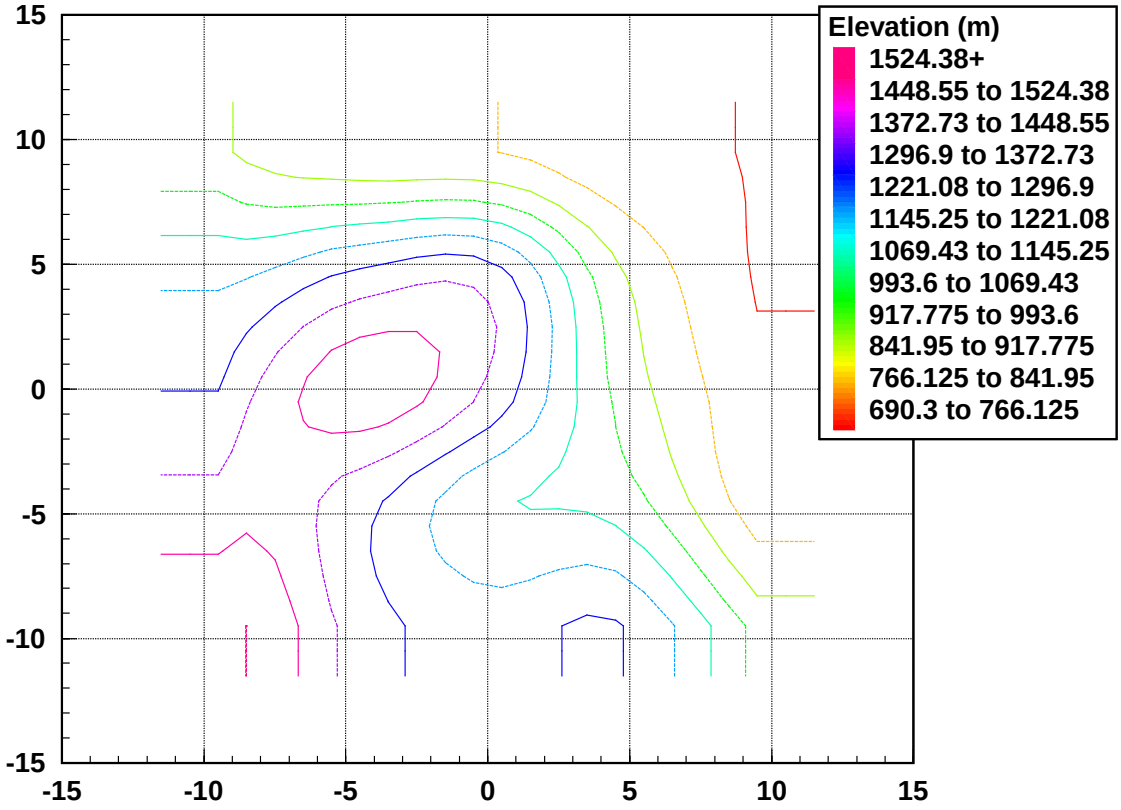

Figure 7 - Contour elevation of Sumanik Mountain (left of centre)

On this and the next page, Figure 8 and Figure 9, show the vertical wind speed in the second and the sixth hour of the RAMS model simulation.

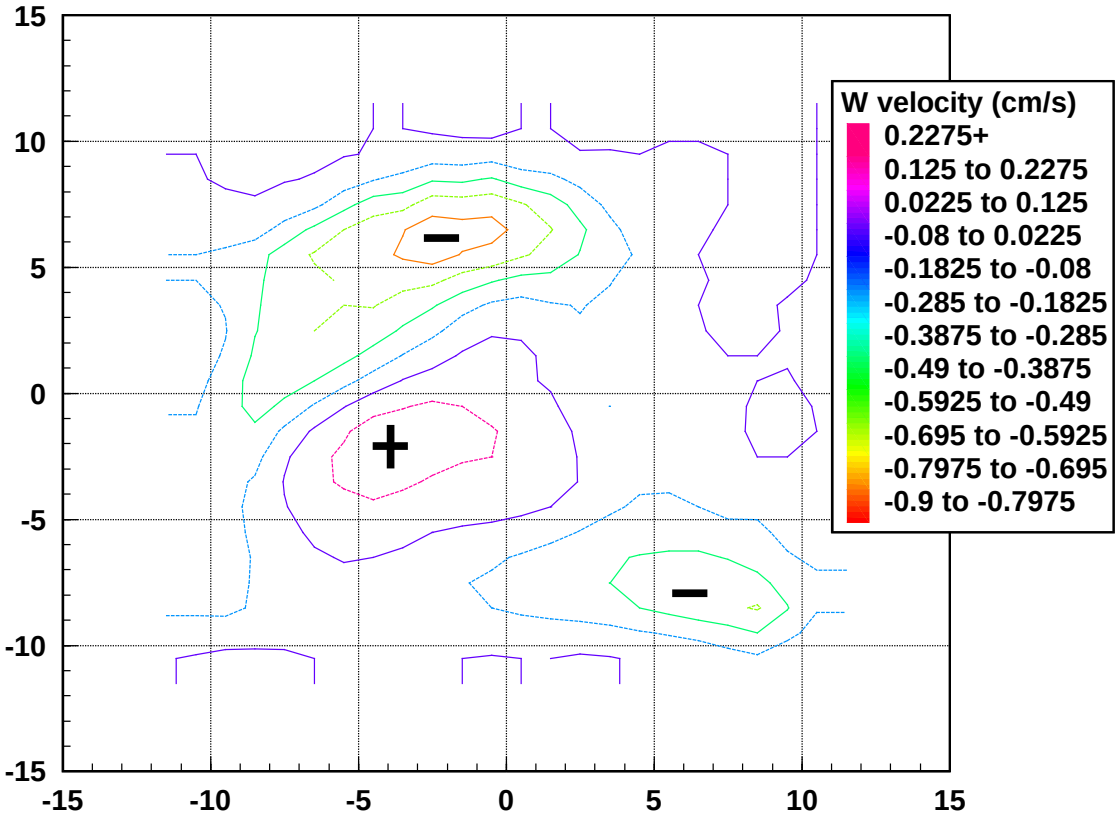

Figure 8 - Vertical speed w after 2 hours

The positive sign in the figure above depicts an upward vertical velocity, which is occurring on the south-east flank of the hill as seen in the previous figure.

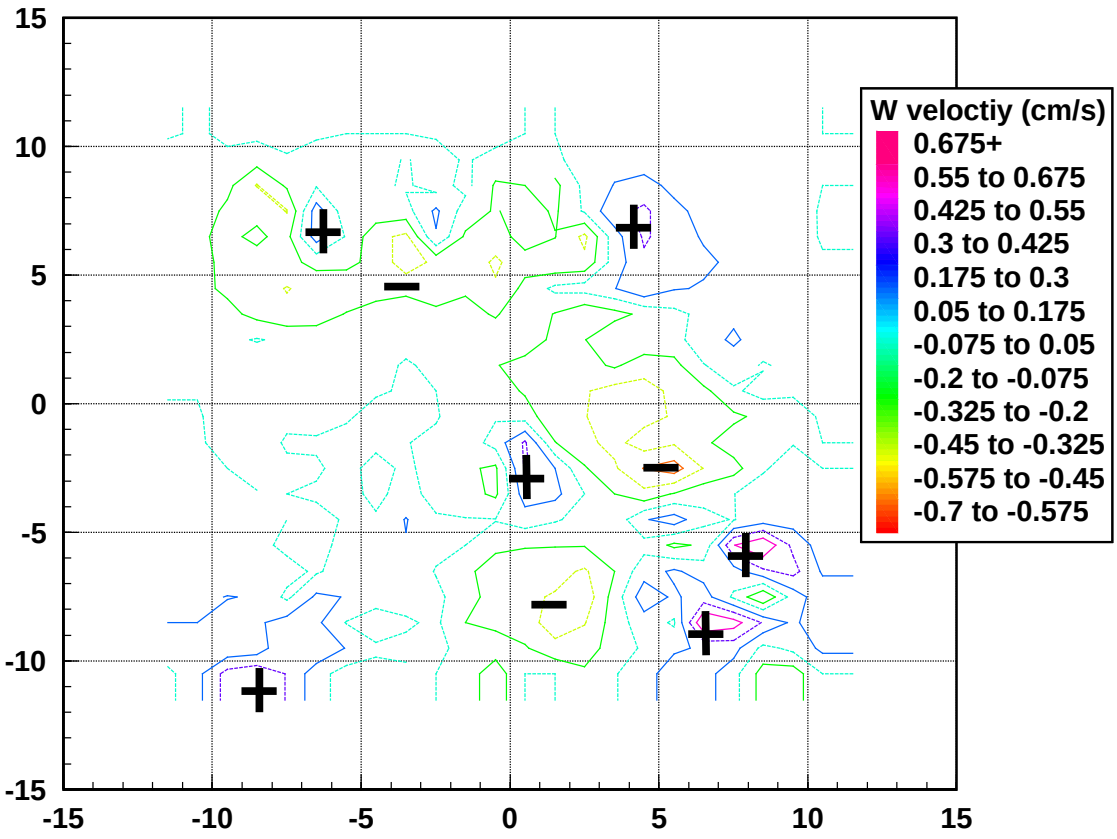

Figure 9 - Vertical speed w after 6 hours